Nanoscale Advances

ROYAL SOCIETY OF CHEMISTRY

REVIEW

View Article Online
View Journal | View Issue

Cite this: *Nanoscale Adv.*, 2025, **7**, 4780

Recent advances in graphitic carbon nitride-based composites for enhanced photocatalytic degradation of rhodamine B: mechanism, properties and environmental applications

Meie Zheng,† Mengru Guo,† Fei Ma, * Wenwen Li and Yujia Shao

Graphitic carbon nitride (g-C_3N_4), a photocatalyst responsive to visible light, shows remarkable promise for the effective photocatalytic decomposition of organic dyes. This can be attributed to its merits, such as low preparation cost and high stability. The synthetic dye Rhodamine B (RhB) poses serious ecological and health risks because it persists in aquatic environments because of its resistance to natural degradation. The purpose of this paper is to review the current breakthroughs in g-C_3N_4 modification. The main methods include surface functionalization and morphological engineering to increase visible light acquisition, suppress charge recombination, enhance visible-light absorption and optimize photocatalytic efficiency. An in-depth analysis of the key factors affecting the degradation of RhB by g-C_3N_4, including the catalyst dosage, solution pH, dye concentration, light conditions, catalyst stability and reusability, was performed. Mechanistic aspects highlight the key role of reactive oxygen species as well as interfacial charge transfer pathways in the system. Finally, to advance the use of g-C_3N_4-based photocatalysts in sustainable environmental remediation, future directions for material optimization and industrial applications are proposed.

Received 4th May 2025
Accepted 26th June 2025

DOI: 10.1039/d5na00439j

rsc.li/nanoscale-advances

1. Introduction

Environmental pollution, especially water pollution, triggered by the industrial wave of globalization has become one of the bottlenecks to sustainable development. Among them, organic dyes pose a long-term and serious threat to the environment because they are not easily degradable. Rhodamine B (RhB) is widely used in a variety of industries, such as textiles, printing, and cosmetics,[1] but owing to its extremely high stability and water solubility, it can continue to accumulate in the environment, causing significant visual pollution and potential ecological harm to water quality.[2] With increasing awareness of environmental protection, the search for efficient, clean, and sustainable organic dye degradation technologies,[3,4] especially for the treatment of difficult-to-degrade pollutants such as RhB, has become an important issue in environmental protection and scientific research.

Photocatalytic technology, with its unique advantages, such as no need for external energy and no secondary pollution, has gradually emerged as a promising technology, especially within the realm of pollution control and treatment.[5–7] Among photocatalysts, g-C_3N_4, as an emerging semiconducting catalyst,[8] has shown great potential for environmental remediation owing to its singular 2D layered structure, excellent thermal stability (600 °C in air), efficient photovoltaic conversion and excellent sensitivity to visible light, and it has rapidly attracted extensive attention from the scientific research community.[9] Given that g-C_3N_4 exhibits a band gap width close to 2.7 eV, it is capable of effectively using sunlight in photocatalytic reactions, thus rendering it an ideal photocatalytic material.[10] However, pure g-C_3N_4 also has inherent limitations, such as a relatively high rate of electron–hole complexation,[11] a restricted spectral response range, and so on, limiting its energy efficiency for practical applications.[12] Therefore, exploring g-C_3N_4-based composites by constructing heterojunctions,[13] surface modification, doping, *etc.*,[14] to increase the overall performance of materials has become a key direction for overcoming these challenges.

Although a number of reviews have explored the wide range of applications of g-C_3N_4-based composites in photocatalysis, the present review focuses on recent progress in the degradation of RhB, a specific and recalcitrant model pollutant, systematically integrates the material design strategies and synergistic mechanisms of g-C_3N_4 in the cross-cutting areas of photocatalytic RhB catalysis, CO_2 reduction, wastewater treatment, and hydrogen energy generation and provides an in-

Hubei Key Laboratory of Resource Utilization and Quality Control of Characteristic Crops, College of Life Science and Technology, Hubei Provincial Engineering Research Center of Key Technologies in Modern Paper and Hygiene Products Manufacturing, School of Mechanical Engineering, Research Center of Hubei Small Town Development, Hubei Engineering University, Xiaogan 432000, China. E-mail: 376144258@qq.com

† These authors contributed equally to this work and share first authorship.

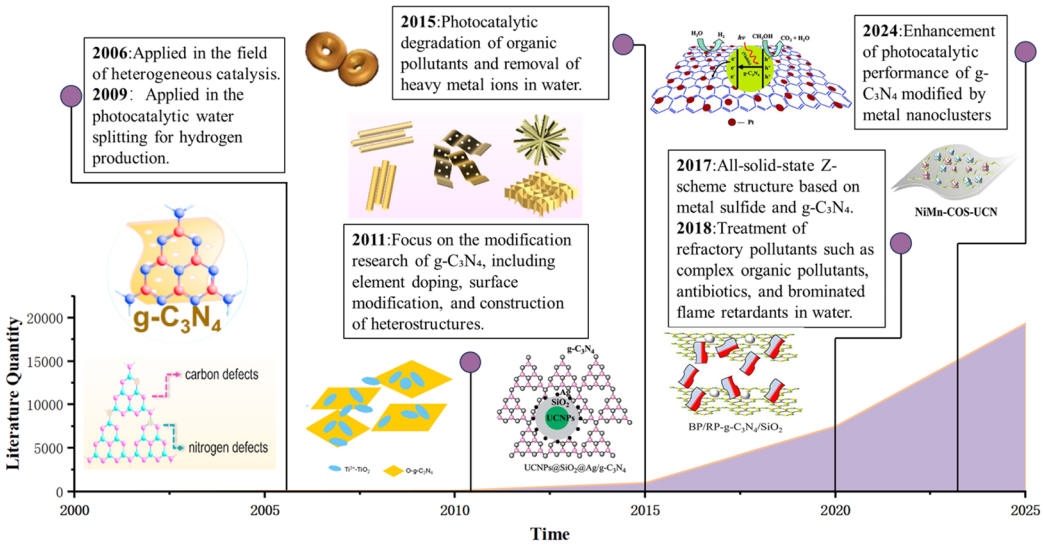

Fig. 1 The development history of g-C_3N_4.

depth analysis of the photocatalytic degradation mechanisms, especially the complex degradation pathways and intermediates of RhB, the principles behind key performance property enhancement, and the potential and key challenges of these composites in practical environmental remediation applications, aiming to provide a comprehensive, timely, and application-oriented knowledge update on g-C_3N_4-based composite research from fundamental mechanisms to environmental applications specifically targeting the highly efficient removal of RhB, thus distinguishing itself from broader thematic reviews and highlighting its unique value and innovative perspectives in addressing specific water pollution problems.

This paper reviews a series of breakthroughs made with respect to the degradation properties of g-C_3N_4 matrix composites for RhB. This approach covers researchers' careful design to effectively improve the photocatalytic efficiency, stability and selectivity of materials, showing their great potential in practical applications[15] and dissecting the working mechanism behind them. These achievements have not only expanded the application scope of g-C_3N_4 but also injected new vitality into environmental protection technology. However, many challenges, including how to further increase the efficiency of light absorption of the material, improve the electron transport speed, and ensure the durability of the material in complex environments, remain to be overcome (Fig. 1).

2. Modification of graphitic carbon nitride

Compared with other common catalysts, g-C_3N_4 is a non-poisonous, extremely plentiful and inexpensive material that has the property of being metal-free.[16] Carbon nitride (CN) was first studied in detail as early as 1996 by two scholars, David M. Teter and Russell J. Hemley, who predicted the cubic form of CN (with a band gap energy of approximately 4.30 eV) through rigorous principle-oriented computations of the comparative stability, structure, and fundamental physical properties of the CN polycrystalline species and reported five types of molecular configurations: β-C_3N_4, α-C_3N_4, p-C_3N_4,g-C_3N_4, and c-C_3N_4.[17] Among such materials, g-C_3N_4 remains the most stable under room-temperature and standard-pressure conditions, has the lowest density, and has been used in many applications, including photocatalysis, gas storage, carbon dioxide reduction, and hydropyrolysis systems.[18,19] Functioning as a catalyst, g-C_3N_4 possesses a band gap energy of 2.65 electron volts. This property allows it to efficiently and directly assimilate light in the visible range of the 400–800 nm range.[20] Furthermore, the redox capacity and excellent chemical stability of the transferred photoexcited carriers make them potentially promising for applications in terms of solar energy conversion and pollutant degradation. For the purpose of boosting the performance of graphite-phase carbon nitride, it can be modified *via* elemental doping, morphology modification, semiconductor compounding, and surface modification (Fig. 2).

2.1. Elemental doping

Elemental doping is a simple and effective method to improve the photocatalytic activity of g-C_3N_4, including metallic and non-metallic elemental doping. For different types of metal oxides, including ZnO, SnO_2, CeO_2, MnO_2, MoO_3, Co_3O_4, Cu_2O and Bi_2O_3, the photocatalytic efficiency of g-C_3N_4 can be enhanced by minimizing electron–hole recombination and facilitating carrier separation.[23] In g-C_3N_4 metal oxide photocatalysts, there exist five kinds of carrier separation mechanisms: Schottky connections, type I hetero-connections, type II hetero-connections, p–n hetero-connections and Z-scheme hetero-connections. The majority of g-C_3N_4 metal oxide photocatalysts display charge carrier separation mechanisms of type II and type Z.[24] Zheng and colleagues used a facile high-temperature synthesis method to dope copper, zinc, manganese and other metal elements into g-C_3N_4 and subsequently

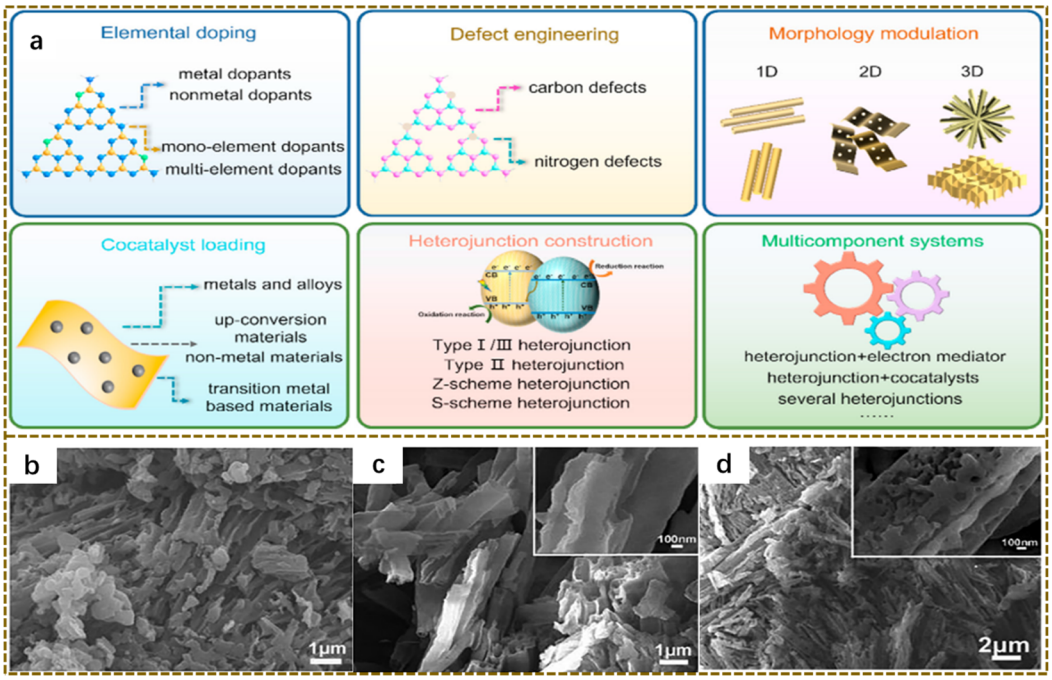

Fig. 2 (a) Design strategy for photocatalysts with g-C_3N_4 as the base material.[21] SEM images of g-C_3N_4 samples with different morphologies: (b) nanoflakes, (c) nanotubes, and (d) rod-like structures.[22]

embedded one-dimensional nanofibrillar fibrillar cellulose (CNF) into the two-dimensional g-C_3N_4 structure. The results of this study revealed a vacuum-assisted filtration technique to prepare manganese-doped g-C_3N_4 photocatalytic composite films presenting a contracted band gap and a broadened region of visible light assimilation, achieving a degradation efficiency of 42.6% within 7 h.[25]

Nonmetallic oxide doping is performed by introducing nonmetallic oxides into the lattice structure of g-C_3N_4, thus modifying its electronical configuration and optoelectronic characteristics. Such dopants can form new energy band structures, expand the range of light absorption, and promote the separation and transport of photogenerated electron–hole pairs. Commonly used nonmetallic oxide dopants include silicon dioxide (SiO_2), aluminum oxide (Al_2O_3), and titanium dioxide (TiO_2). The applications of nonmetallic oxide-doped g-C_3N_4 cover a wide variety of aspects like the photocatalytic removal of organic pollutants through catalytic reaction under light, the hydrogen generation *via* photocatalysis, and the CO_2 reduction through photocatalysis. The photocatalytic performance and application effect could be further enhanced by optimizing the doping ratio and manufacturing method. Xiao *et al.* employed thiourea and melamine as starting materials and utilized a one-step calcination process to fabricate highly active sulfur-doped porous g-C_3N_4 materials (labeled C_3N_4–S). Under visible light irradiation, C_3N_4–S demonstrated remarkable photocatalytic capabilities for the decomposition of RhB. The material significantly enhances the electron transfer efficiency and effectively improves the separation of photogenerated electron–hole pairs, thus substantially enhancing the photocatalytic efficiency.[26]

2.2. Composite semiconductor

The rapid rate of charge complexation during the fast charging process and the poor response to visible light are the primary limitations that constrain the photocatalytic performance of g-C_3N_4.[28] Combining g-C_3N_4 with semiconductors to construct composites has been demonstrated as an efficient approach to enhance the photocatalytic activity of g-C_3N_4.[29] Using a single-step ball milling technique, Li *et al.* constructed a type II heterojunction at the g-C_3N_4/BP/RP interface, synthesizing the BP/RP-g-C_3N_4/SiO_2 material. This heterojunction significantly enhanced the separation of photogenerated carriers and the electron transfer efficiency. Under simulated solar radiation for just 26 min, the material achieved 90% RhB degradation, which was 1.8 times better than that of g-C_3N_4/SiO_2 (Fig. 3b).[27]

2.3. Surface modification

Surface modification is a significant means to improve the efficiency with which g-C_3N_4-based photocatalysts remove pollutants. By modifying the functional groups that are present on the surface of the catalyst, surface active sites and carrier kinetics can be effectively regulated, and the relationship between structure and performance can be explored in detail. Liu *et al.* prepared halide ion surface-modified CN materials (denoted as CN-X) by simple room temperature (25 °C) impregnation of g-C_3N_4 with a dilute aqueous solution of hydrohalic acid (HX, where X stands for F, Br and Cl), which brought about a notable enhancement in the photocatalytic degradation process of RhB and phenol, in addition to the generation of hydroxyl radicals (OH) compared with unmodified CN.[30] The coupling of g-C_3N_4 with other materials can be

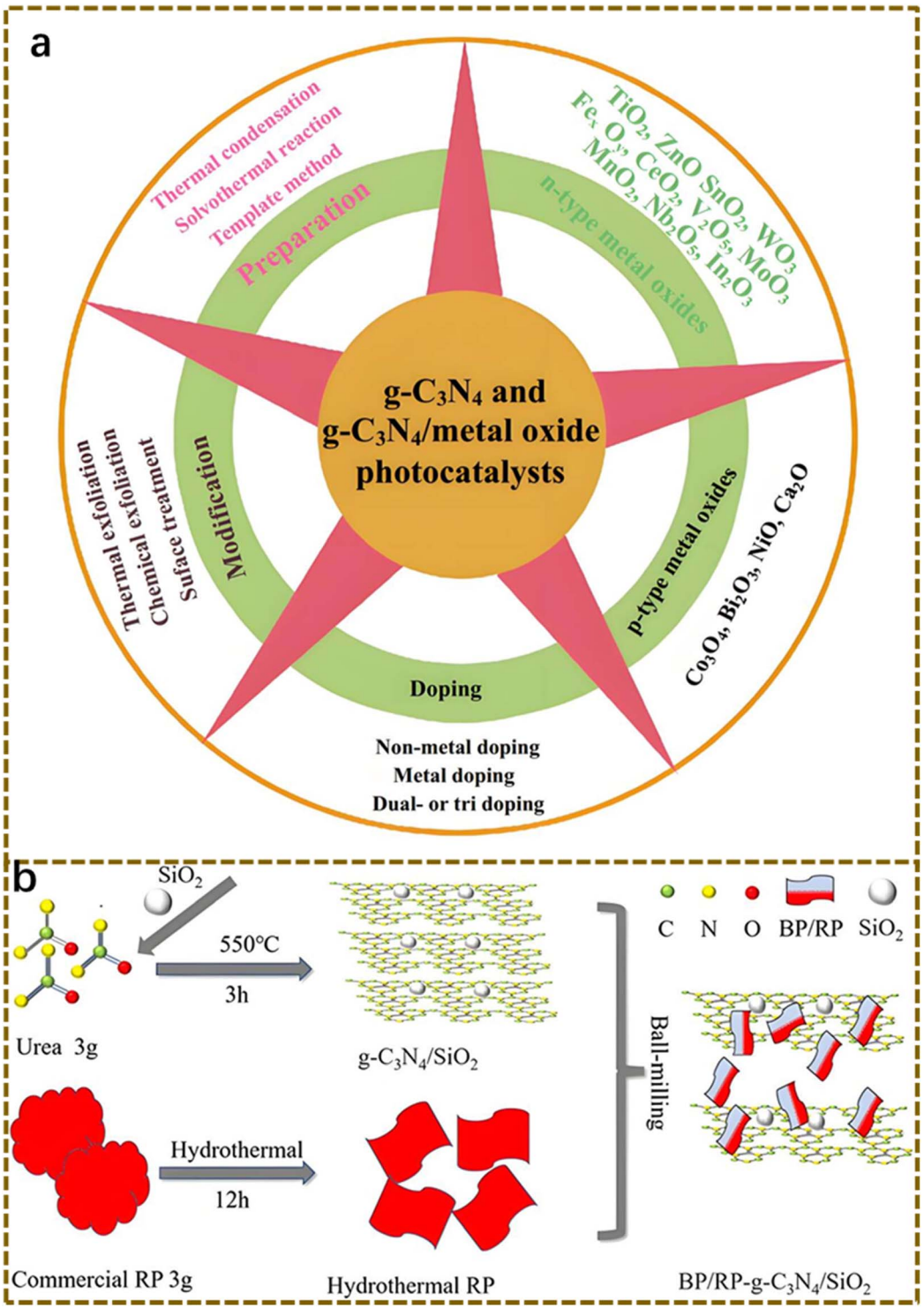

Fig. 3 (a) The g-C_3N_4 and g-C_3N_4/metal oxide photocatalysts: schematic representation.[23] (b) Diagram presenting the procedure for preparing the BP/RP-g-C_3N_4/SiO_2 photocatalyst in a schematic way.[27]

carried out by covalent modifications (covalent bonding or p–p stacking interactions) and noncovalent modifications.[31–33] Sun *et al.* reported that monoatomic cobalt-doped g-C_3N_4 enhanced surface charge separation and hydrogen peroxide production.[34]

2.4. Morphological control

To improve the degradation efficiency, shape regulation is another efficient approach, since it can effectively address the limitations of g-C_3N_4, such as its inherently restricted specific surface area and the swift recombination rate of photo-induced

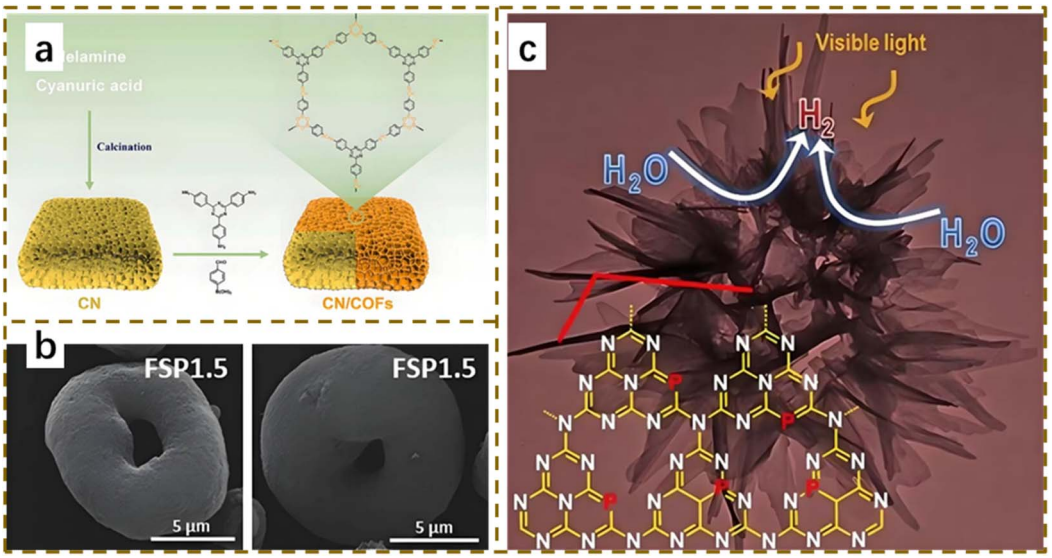

Fig. 4 (a) Modifying spongy g-C_3N_4 with covalent organic frameworks (COFs).[38] (b) Torus-shaped g-C_3N_4 particles prepared using the flame spray pyrolysis (FSP) technique.[39] (c) Used for hydrogen production *via* water photolysis, the flower-like nanostructure of phosphorus-doped g-C_3N_4.[40]

carriers, and subsequently improve its adsorption capacity for light energy and pollutants.[35] A newly-developed method for making graphitic carbon nitride (TUM-CN-2) with a rectangular hollow tube structure and rough surface created by means of the self-assembly of hydrothermal products from the combination of urea and melamine with trithiocyanuric acid was developed by Deng *et al.* The produced photocatalyst TUM-CN-2 showed a 13.96-fold increase in RhB degradation efficiency under irradiation under visible-spectrum light in comparison with that of pure g-C_3N_4.[36] In an additional study, Wang *et al.* successfully prepared petal-like chlorine-introduced graphitic phase g-C_3N_4 nanosheets *via* a self-assembly technique with melamine as a precursor, and the prepared chlorine-doped g-C_3N_4 nanosheets removed 94.3% of RhB in 90 min, with a degradation kinetic rate 15.8 times higher than that of original g-C_3N_4, it was 15.8-fold higher, demonstrating significantly improved efficiency (Fig. 4).[37]

As a nontoxic, inexpensive and abundant metal-free photocatalytic material, g-C_3N_4 has potential applications in photocatalysis and solar energy conversion because of its 2.65 eV bandgap, which enables response to 400–800 nm visible light. However, the problems of fast photogenerated carrier

Table 1 Strategies for enhancing charge carrier separation in g-C_3N_4-based photocatalysts

Strategy	Modification approach	Photocatalytic performance	Mechanism	Ref.
Morphological engineering	Solvothermal exfoliation into 1D nanotubes & 2D nanosheets using a H_2O_2-mediated process	547% higher photocurrent, 220% faster Congo red degradation, and 180% faster tetracycline removal	Increased surface area, enhanced charge transport, and reduced recombination	Panchu[41]
Heteroatom doping	Dual P-doping in the g-C_3N_4 framework	Improved H_2O_2 production efficiency, and higher charge dissociation	Modified electronic structure and reduced exciton binding energy	Yu[42]
Defect engineering	Introduction of N vacancies and cyano groups *via* alkali etching	Enhanced O activation, improved $^{\bullet}O_2^-$ and $^1O_2$ generation	Facilitated charge transfer and improved oxygen adsorption	Zhang[43]
Heterojunction construction	g-C_3N_4/$MnIn_2S_4$ heterostructure	92.3% RhB and 72.8% TC degradation under visible light	Type-II band alignment and efficient electron–hole separation	Xiao[44]
Crystalline film growth	CVD-grown crystalline g-C_3N_4 thin films with sulfur doping	Extended carrier lifetime (12.43 ns), and a tunable bandgap (3.05 eV)	Improved crystallinity and enhanced charge mobility	Du[45]
Dual functionalization	Hydroxyl and π-rich electron domains in g-C_3N_4	Boosted H_2O_2 production without sacrificial agents	Enhanced exciton dissociation and selective reactant adsorption	Shen[46]
Ternary heterojunction	g-C_3N_4/BiOBr/$Bi_2O_2CO_3$ for Zn-air batteries	Improved ORR/OER kinetics and photo-assisted charging efficiency	Efficient charge separation and visible-light-driven redox reactions	Khampuanbut[47]

recombination and limited specific surface area constrain its performance. Currently, modification research has been optimized through elemental doping, semiconductor compounding, surface modification and morphology modification: elemental doping adjusts the energy band structure by introducing metallic or nonmetallic elements to promote carrier separation; compounding with semiconductors builds heterojunctions to accelerate carrier migration; surface modification modifies the functional groups to regulate the surface active sites and improve the efficiency of charge separation; and morphology modification increases the specific surface area and photocatalytic properties through the preparation of hollow tubes, nanosheets and other structures to increase photovoltaic conversion and light absorption. By synergistically optimizing the energy band structure, carrier transport and surface properties, these modification strategies provide an opportunity to explore the synergistic principles of cross-scale modification mechanisms, establish an integrated optimization system from atomic structure design and energy band engineering to surface interface reactions, and promote the practical application of g-C_3N_4-based materials in the fields of sustainable energy and pollution control (Table 1).

3. Research on the degradation traits of g-C_3N_4 composite materials

3.1. Comparison of RhB degradation efficiency across different composite materials

In recent years, g-C_3N_4-based magnetic photocatalysts have exhibited significant potential for water purification, and consequently, they have been receiving more and more attention from the academic community. Among various pollutants in the environment, RhB is a common alkaline organic pollutant, and a synthetic dye with a bright peach color; thus, it has been widely used in the textile dyeing, papermaking and printing, and cosmetic industries. However, the conjugated system and cationic properties of the molecular structure of RhB make it highly stable in the environment and difficult to decompose *via* natural processes. Karimzadeh and Shariatinia fabricated ZIF-8/OH-g-C_3N_4/$La_2Sn_2O_7$ nanocomposites. Under visible light, the binary composite with 10% $La_2Sn_2O_7$ in OH-g-C_3N_4 showed optimal activity. The derived ternary material (10% $La_2Sn_2O_7$/OH-g-C_3N_4)/10% ZIF-8 achieved 97.1% degradation of 10 ppm RhB in 120 minutes at pH = 11 (Fig. 5c), maintaining 80.5% efficiency after five cycles, with the mechanism attributed to a double Z-scheme charge transfer.[48] In order to clearly present the differences in RhB degradation performance of different g-C_3N_4-based composites, the relevant performance disparities are specifically analysed in Table 2.

α-Fe_2O_3/Fe_3O_4/g-C_3N_4 nanocomposites with magnetic separation properties were synthesized *in situ via* the solution combustion method by M. Afkari *et al.* Photocatalytic tests revealed that the type and content of iron oxides significantly affected the visible light decolorization of RhB, with the composite containing 37 wt% iron oxides exhibiting a photodegradation efficiency superior to that of pristine g-C_3N_4.[49] In addition, Soheila Sharafinia *et al.* successfully synthesized a magnetic chalcogenide nanohybrid based on g-C_3N_4 nanosheets by integrating $SrTiO_3$: N (STO : N). Through a facile reflux

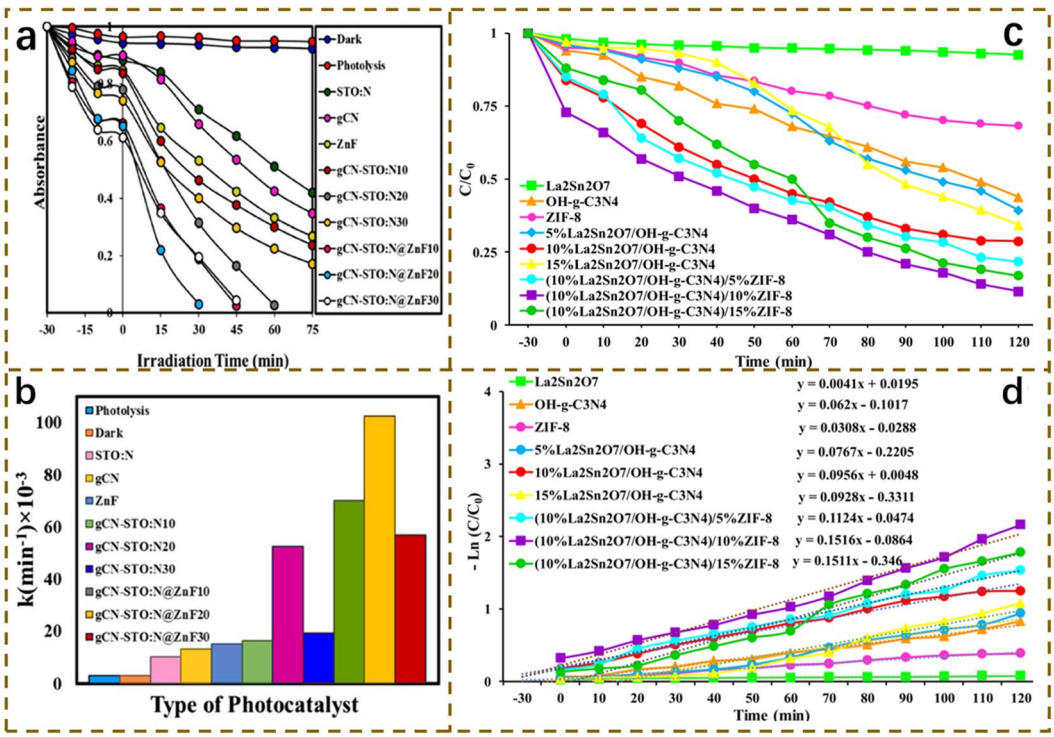

Fig. 5 (a) Light-catalyzed performance of the synthesized extracts in degrading RhB; (b) degradation rate constants of RhB on the synthesized photocatalysts; (c) 0.10 g of various photocatalysts were used to conduct photocatalytic degradation reactions of RhB in water for 120 minutes under both dark and visible light conditions; (d) degradation efficiency of different photocatalysts.[48]

Table 2 Analysis of the degradation performance disparities of different g-C_3N_4-based composite materials for RhB

Materials	Synthesis method used	Photocatalyst dosage	RhB concentration	Light source power	Degradation time	Photodegradation	Ref.
CNT/mp-g-C_3N_4	Refluxing/thermal polymerization	30 mg	10 mg L^{-1}	480 W	300 min	90%	Chen[51]
g-C_3N_4/Fe_3O_4/rGO	Precipitation method				75 min	100%	Luo[52]
g-C_3N_4/$Na_2Ti_3O_7$/V_2O_5	Hydrothermal method	50 mg	20 mg L^{-1}	300 W	60 min	90%	Vattikuti[53]
$CoFe_2O_4$/g-C_3N_4	Sol–gel and ultrasonic treatment	30 mg	20 mg L^{-1}	500 W	120 min	57%	Dharani[54]
f-CNT/PhCN	Water-bath method	4 mg	10 mg L^{-1}	13 W	240 min	60%	Ghourichay[55]
N/$ZnCo_2O_4$/g-C_3N_4	Hydrothermal method	10 mg	20 mg L^{-1}	150 W	60 min	92.34%	Nasir and Alshamsi[56]
g-C_3N_4/NiO/CC	Electrodeposition and calcination	0.1 mg	7 mg L^{-1}	300 W	60 min	98%	Yang[57]
AC/g-C_3N_4	Thermal polycondensation method	100 mg	30 mg L^{-1}	300 W		97%	Shi[58]
Ag/g-C_3N_4	Deposition method	60 mg	20 mg L^{-1}	300 W	60 min	100%	Le[59]
Ag_3PO_4/GO/g-C_3N_4					50 min	94.8%	Yan[60]
Cu^+/g-C_3N_4/Bi_2WO_6	Calcination and solvothermal method	20 mg	20 mg L^{-1}	100 W	50 min	98.46%	Hong[61]
Fe–Mo–O/g-C_3N_4		300 mg	10 mg L^{-1}	300 W	15 min	99%	Kong[62]
Bi_2MoO_6/g-C_3N_4	Eco-friendly ultrasonic-assisted method	100 mg	1 mg L^{-1}	100 W	180 min	94.6%	Masoud[63]
S/P-g-C_3N_4	Secondary calcination modifications	10 mg	30 mg L^{-1}	300 W	4 min	99.4%	Yang[64]
MWCNTs-g-C_3N_4	Electrostatically driven self-assembly with the hydrothermal method	50 mg	10 mg L^{-1}	300 W	180 min	89.7%	Xu[65]
rGO-g-C_3N_4	Thermal treatment	8 mg	5 mg L^{-1}	1000 W	100 min	75%	Li[66]
U Doped g-C_3N_4		10 mg	10 mg L^{-1}	300 W	50 min	100%	Zhan[67]
P-doped g-C_3N_4	The thermal oxidation and element doping associated method	20 mg	20 mg L^{-1}	300 W	70 min	99.5%	Li[68]
Fe-g-C_3N_4	Two-step calcination thermal polymerization				45 min	90%	Ji[69]
K-doped g-C_3N_4/BiOBr	Element doping method	50 mg	20 mg L^{-1}	500 W	90 min	90%	Qu[70]
Ag_{10}–C_3N_4-NA_2SO_4	Deposition method	25 mg	10 mg L^{-1}	350 W	50 min	96.5%	Wang[71]
MIL125(Ti)/g-C_3N_4/rGO	Self-assembled	25 mg	10 mg L^{-1}	32 W	120 min	98%	Fatima and Kim[72]

approach, $ZnFe_2O_4$ (ZnF) was incorporated onto the exterior of g-C_3N_4 nanosheets, and the nanohybrid was capable of efficiently breaking down numerous types of organic colorants, with RhB being one of them, in a short time. The nanohybrid can efficiently degrade a variety of organic dyes, including RhB, in a short period of time, with a degradation efficiency of more than 90%. The nanocomposite containing 20 wt% STO : N chalcogenide and 20 wt% ZnF was able to achieve the highest RhB degradation rate under visible light irradiation in just 30 min (Fig. 5).[50]

3.2. Factors affecting degradation performance

3.2.1. Catalyst dosage. The catalyst dosage is an important factor affecting degradation performance. Within a certain range, the degradation rate of RhB increases as the catalyst dosage increases. However, when the catalyst dosage is too high, the blockage of light by the suspended catalyst particles reduces the utilization of photons, thus decreasing the degradation efficiency. Fe_2O_3/2D-C_3N_4/NiFe-LDH composites were prepared by Mohammadi *et al.* The magnetic material was demonstrated to act as a stable photocatalyst to enhance photocatalytic activity in the breakdown of dyes; with regard to MB and RhB, the maximum elimination efficiencies were 91.2% and 88.5%, respectively. When the initial concentrations of MB and RhB were set at 10 mg L^{-1} and 9 mg L^{-1} respectively, with a catalyst loading of 0.36 g L^{-1}, an initial pH of 9.0, and an LED irradiation time of 60 minutes, 80% of the COD underwent photodegradation under the best-fit conditions.[73]

3.2.2. Initial pH of the solution. The original pH level of the solution also significantly affected the degradation performance. In an acidic environment, the lower the pH is, the faster the degradation rate of RhB. In an alkaline environment, the greater the pH value, the lower the degradation rate. This may be due to the different morphologies and charge states of RhB

molecules at different pH values, which affect their adsorption and reaction with photocatalysts. Vadivu *et al.* fabricated $CaWO_4$/g-C_3N_4 nanocomposites and investigated the effects of various reaction parameters, such as the initial catalyst dosage, pH, contact time and initial dye concentration. Under optimized conditions (specifically, at a pH value of 8), when 80 mg L^{-1} of the $CaWO_4$/g-C_3N_4 nanocomposites containing 3% g-C_3N_4 (CC3) was applied and the concentration of the RhB dye was 7.5 ppm, approximately 98% of the RhB was degraded within 150 minutes.[74]

3.2.3. Dye concentration. The dye concentration is also a factor that affects degradation performance. The photocatalytic reaction slows down as the dye concentration increases. This may be because high concentrations of dye molecules competitively bind to the surface of the photocatalyst, thus reducing the chance of each dye molecule reacting with the photocatalyst. AgI/g-C_3N_4 heterojunctions were prepared in a study by Alsulmi *et al.* Photocatalytic experiments revealed that g-C_3N_4 sheets decomposed 12% of the RhB dye and that the ultrafast rate of electron–hole pair complexation was inhibited owing to the inefficient separation of electron–hole pairs and the limited surface area of the solid sample. Regarding heterojunctions with 5 wt%, 10 wt% and 15 wt% of AgI content, the breakdown of RhB dye was close to 67%, 92% and 85% of the original concentration of the dye, respectively.[75]

3.2.4. Light conditions. The light source conditions also have some influence on the degradation performance. In the case where sunlight was employed as the light source, the g-C_3N_4 catalyst showed a certain decolorization effect on real dye production wastewater. The intensity of sunlight varies across different time periods and weather conditions, thus affecting the degradation efficiency. Moghimifar and colleagues prepared composites that consisted of molybdenum disulfide (MoS_2) and g-C_3N_4. Then, under visible light illumination, they

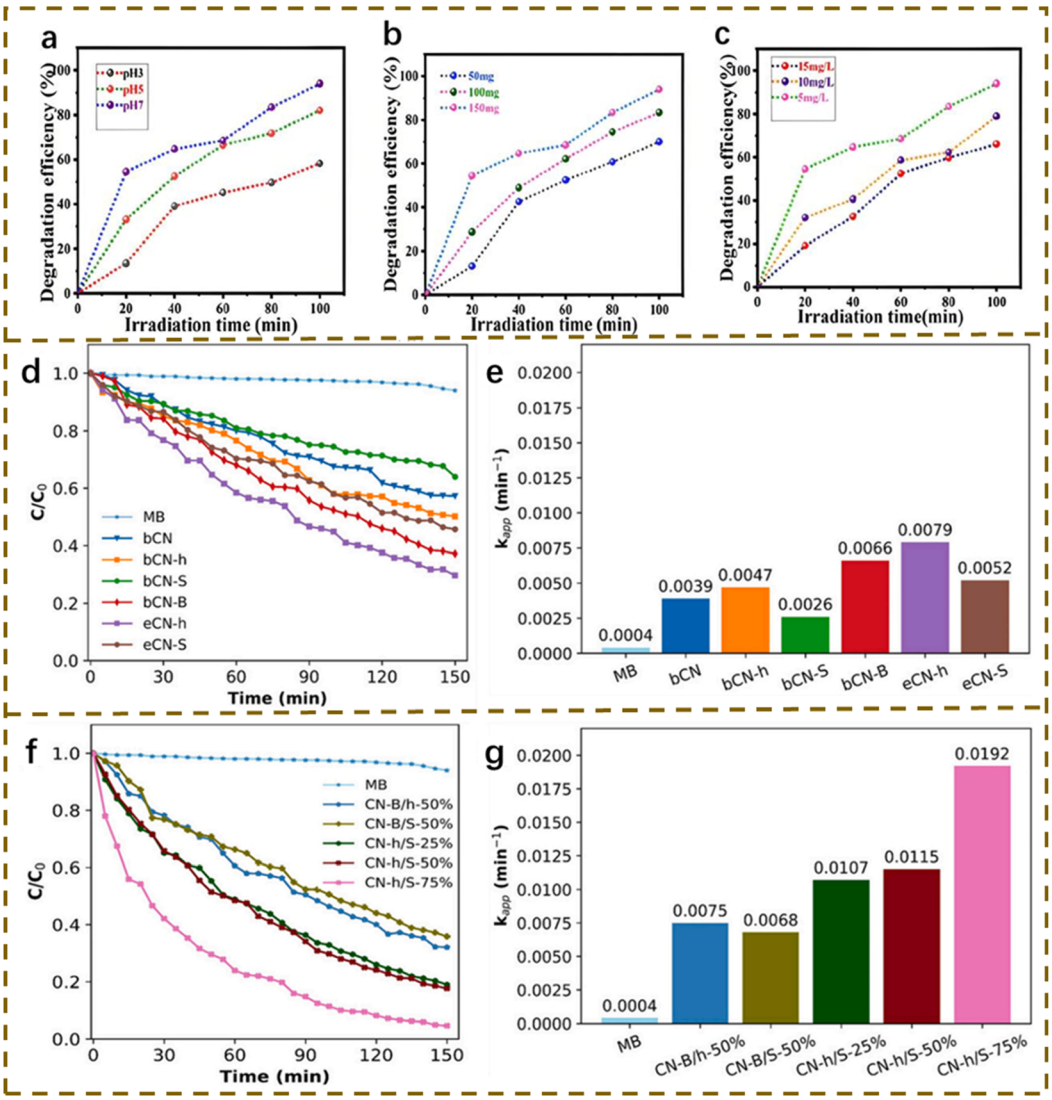

Fig. 6 Effects of (a) pH, (b) catalyst, and (c) dye concentration on RhB degradation performance.[77] (d and e) Catalytic decomposition of methylene blue dye under light irradiation dye under the influence of CN, b-CN-h, b-CN–S, b-CN–B, e-CN-h, and e-CN-S, as well as their reaction rate constants (K_{app}). (f and g) Degradation of methylene blue dye by heterojunctions and their K_{app}.[78]

verified the photocatalytic properties of the MoS_2/g-C_3N_4 composite *via* the decolorization process of RhB. They experimentally demonstrated that parameters such as exposure time, photocatalyst concentration and the percentage of triethanolamine (TEOA) functioning as a sacrificial agent have an impact on the efficiency of the hydrolysis reaction.[76]

3.2.5. Methods of preparation and structures of composite materials. The preparation method and structure of the composite also affect its degradation properties. By optimizing the preparation method and adjusting the structure of the composites, their specific surface area and light absorption properties can be improved, thus increasing the photocatalytic degradation efficiency (Fig. 6).

3.3. Effect of recycling on degradation properties

In commercial wastewater treatment, the recoverability and reuse of catalysts play key roles in enhancing the competitiveness of the process. The g-C_3N_4 photocatalyst (UCN) prepared by Zhang *et al.* using urea as a starting material exhibited superior photocatalytic properties, accomplishing 99.61% removal within 40 minutes. The UCN photocatalyst, moreover, was capable of fully degrading 10 mg L^{-1} RhB dye within 20 minutes under sunlight. Its excellent stability and reusability were demonstrated by the fact that the degradation rate stayed above 99% even after four cycles.[79] In another study, Soheila Sharafinia, along with her team, fabricated a magnetic chalcogenide nanohybrid based on g-C_3N_4 nanosheets. They achieved this by integrating STO : N and ZnF onto the g-C_3N_4 nanosheets through the refluxing technique; the nanohybrid showed exceptional stability and reusability over seven uninterrupted experiments, and its significant photocatalytic activity was retained even after numerous degradation cycles. Its high photocatalytic activity was still maintained. They demonstrated that because of the strong interaction between the magnetic chalcogenide component and the g-C_3N_4 nanosheets, the material didn't aggregate and could be used efficiently.[50] In addition, $BiVO_4$ nanocomposites (10 wt% g-C_3N_4@$BiVO_4$ and 5 wt% g-C_3N_4@$BiVO_4$) containing g-C_3N_4 were prepared *via* the wet immersion method by Priti Rohilla *et al.* Under visible light irradiation, the RhB degradation efficiency of the 10 wt% g-

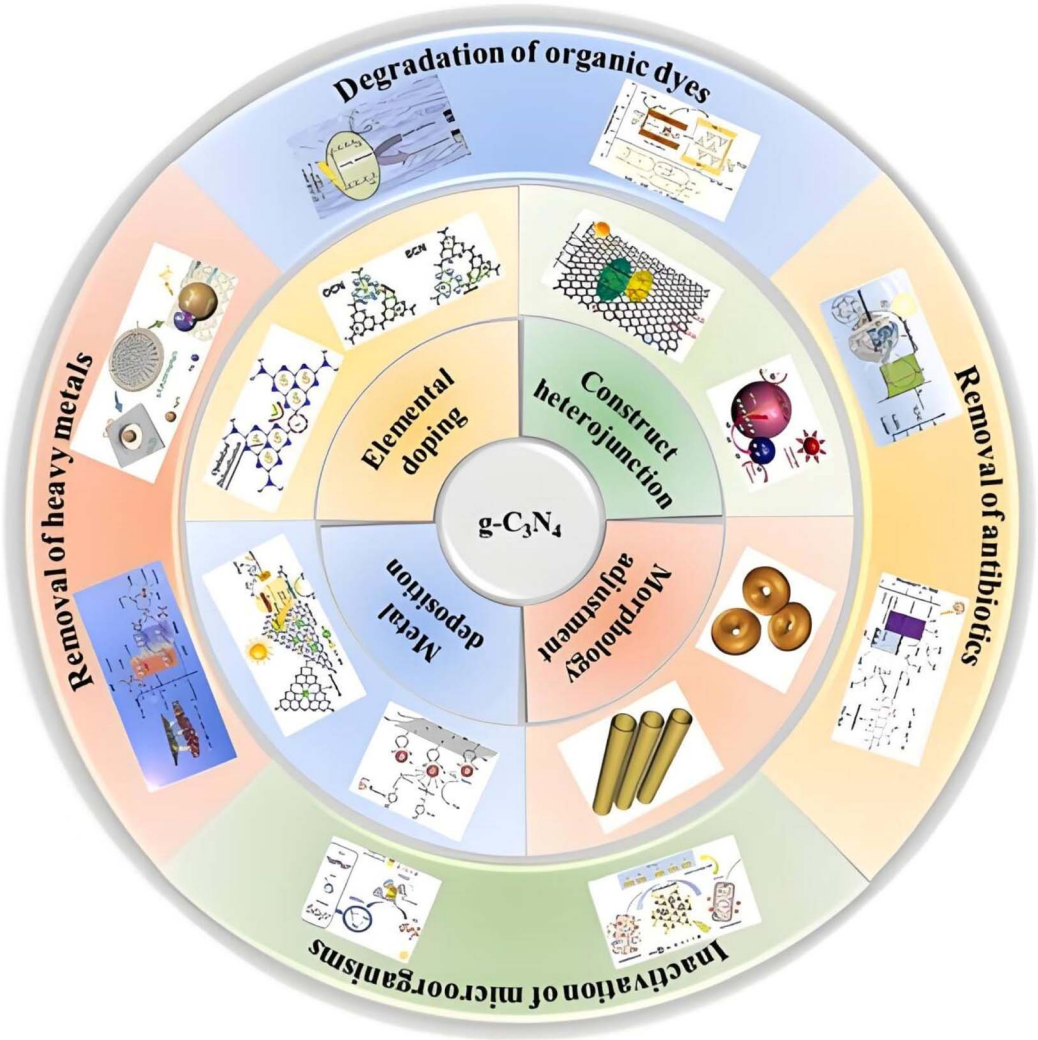

Fig. 7 Designing and modifying g-C_3N_4.[82]

C_3N_4@$BiVO_4$ composites reached 86% after 60 min of reaction, as they presented the best catalytic activity. The stability of the heterostructures was confirmed by the fact that their photocatalytic activity decreased by only 14% even after five cycles.[80] Xu *et al.* loaded $BiVO_4$ onto protonated g-C_3N_4 *via* an electrostatic self-assembly method and then constructed a novel ternary $BiVO_4$/protonated g-C_3N_4/AgI photocatalyst with a double Z-type mechanism *via* an *in situ* precipitation route. After 60 min of visible-light irradiation, this led to a RhB removal rate of 94.67% and a photodegradation rate constant of 0.04963 min^{-1}, which was higher than those of pristine $BiVO_4$ (0.0004 min^{-1}), $BiVO_4$/protonated g-C_3N_4 (0.0209 min^{-1}) and $BiVO_4$/AgI (0.0317 min^{-1}). The synthesized ternary samples demonstrated excellent stability following four cycles of photodegradation.[81]

3.4. Methods to boost stability

The stability and reusability of g-C_3N_4 composites for RhB degradation can be remarkably enhanced by surface modification, composite construction, preparation process optimization, and posttreatment and regeneration methods. These strategies provide strong support for the utilization of g-C_3N_4 composites in photocatalysis (Fig. 7).

g-C_3N_4 matrix composites have shown significant advantages in the field of RhB degradation. Nevertheless, there is still room for improvement in their practical applications. The degradation efficiency of some composites decreases with increasing concentrations of RhB or complex water, and interfacial engineering is needed to increase the adsorption capacity and solve the problem of light shielding. The activity decay during long-term cycling reveals insufficient interfacial bonding, and the intercomponent interactions need to be strengthened. The current preparation process is complicated and costly, and a green and low-cost pathway should be developed. Challenges such as pH fluctuations and competitive adsorption of coexisting pollutants in real wastewater treatment require a synergistic transformation of material design toward anti-interference and multifunctionality while deepening mechanistic research to support the construction of efficient heterogeneous structures.

4. Study of the degradation mechanism of g-C_3N_4 composites

4.1. Photocatalytic mechanism

On the basis of the principle of photocatalytic degradation, researchers have developed a series of improved g-C_3N_4 nanocomposites aimed at solving the problems of traditional catalysts and successfully realizing the rapid and effective degradation of organic contaminants. These improvements include the incorporation of metallic substances and nonmetallic elements, combination with other semiconducting materials, fine tuning of the material morphology, codoping of multiple elements, and immobilization of the material on a carrier (Fig. 8).

Metal doping, nonmetal doping, and combining with other semiconductors all significantly boost the efficiency of the catalysts. For instance, the combination of two π-conjugated systems, g-C_3N_4 and BiOBr, effectively increases the degree of charge separation for electrons and holes within an individual material, while also enhancing the extent of the solar spectrum that can be efficiently utilized.[83] The band gap of g-C_3N_4, an important semiconductor material, is 2.65 eV. Notably, its valence band (VB) potential is 1.56 eV and conduction band (CB) potential is −1.09 eV, respectively.[84] When g-C_3N_4, a well-known semiconductor material, absorbs a high electronic photon with an energy of no less than 2.65 eV, electrons residing in the VB rapidly transfer to the CB. Simultaneously, holes are generated in the VB. Moreover, given that the electrons have a potential as low as −1.09 eV, dissolved oxygen (DO) in the surrounding environment can readily react with them. This reaction efficiently gives rise to superoxide radicals ($^{\bullet}O_2^-$), which, in turn, can effectively serve as reactive agents for degrading various pollutants.[22] By using RhB as an illustration, the reaction process of this system can be clearly depicted in the following way:

$$\text{g-}C_3N_4 + h\nu \rightarrow e_{CB}^- + h_{VB}^+ \quad (1)$$

$$O_2 + e^- \rightarrow {}^{\bullet}O_2^- \quad (2)$$

$$H_2O + h_{VB}^+ \rightarrow {}^{\bullet}OH + H^+ \quad (3)$$

$$RhB + h_{VB}^+/O_2^-/OH \rightarrow \text{intermediates} \rightarrow CO_2 + H_2O \quad (4)$$

During photocatalytic degradation, the types of reactive oxygen species (ROS) produced by g-C_3N_4 composites and their generation mechanisms are crucial for understanding their catalytic mechanism. In addition to $^{\bullet}O_2^-$, g-C_3N_4-based composites can generate a variety of reactive species, such as $^{\bullet}OH$ and single-linear oxygen ($^1O_2$), under light conditions. Among them, $^{\bullet}O_2^-$ is generated mainly by the reaction of conduction band electrons (e^-) with dissolved oxygen, whereas $^{\bullet}OH$ is produced by the direct oxidation of surface adsorbed water or hydroxyl groups *via* valence band holes (h^+). Notably, the pathways and proportions of ROS generation can be significantly altered by constructing heterojunctions or through elemental doping. For example, in the g-C_3N_4/BiOBr heterojunction system, the formation of a type II heterojunction due to energy band matching promotes charge space separation, resulting in a significant increase in the $^{\bullet}O_2^-$ yield, whereas sulfur-doped g-C_3N_4 is more favorable for $^{\bullet}OH$ generation because of a positive shift in its valence band position.

Differences in interfacial charge transfer pathways directly affect the photocatalytic efficiency. In g-C_3N_4-based composites, there are three main typical charge transfer mechanisms: in metal-doped systems, the metal atoms may act as electron trapping centers to promote charge separation; in semiconductor composite systems, the construction of type II, Z, or S heterojunctions creates different charge transfer pathways; and in carbon quantum dot-modified g-C_3N_4, the electron storage-release mechanism may prolong the lifetime of the carrier.

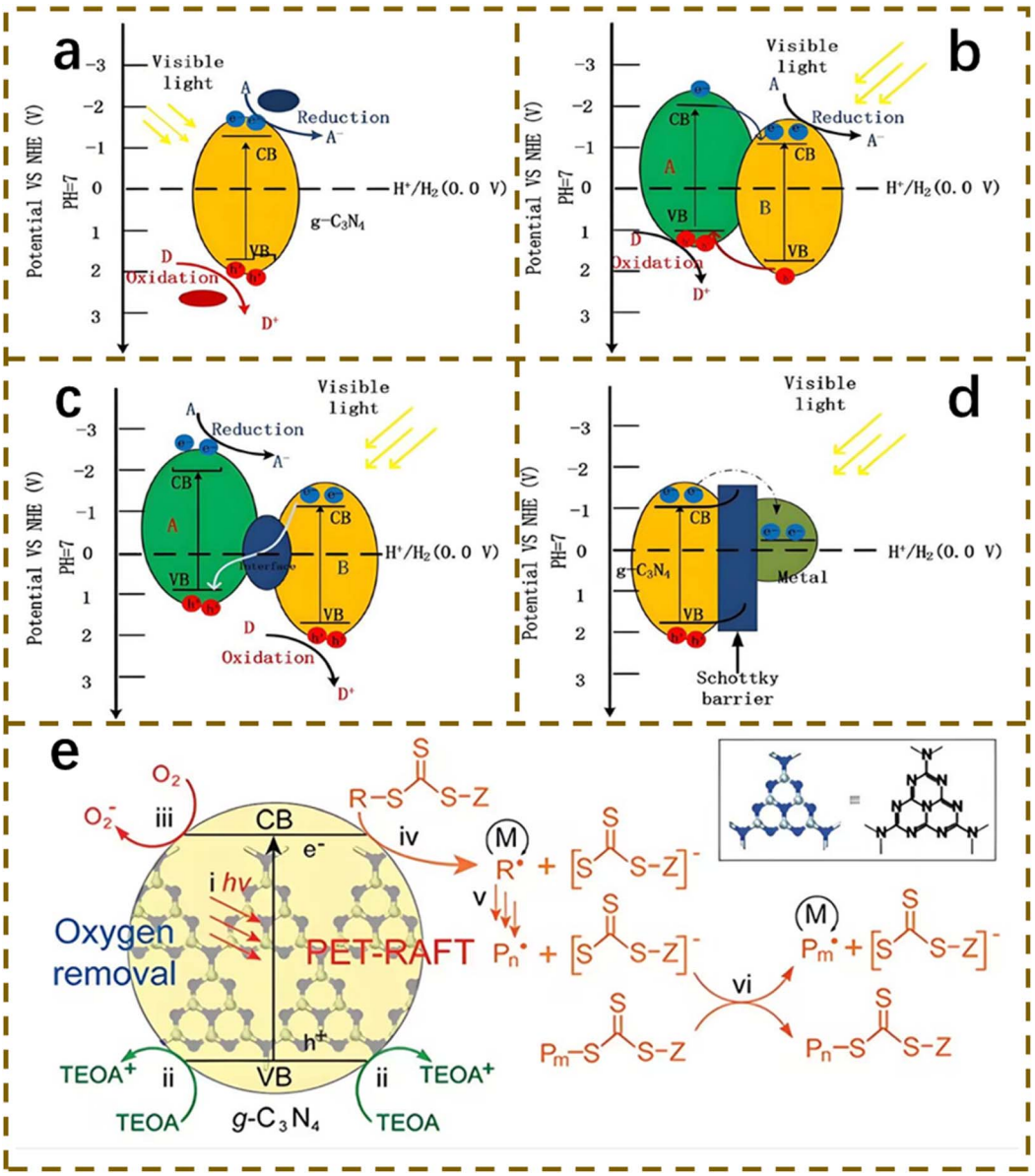

Fig. 8 (a) The characteristic photocatalytic mechanism of pristine g-C_3N_4; (b) the schematic illustration of photoinduced charge migration in a type II heterojunction; (c) the Z-scheme heterojunction configuration; (d) the Schottky junction structure;[85] (e) the photoinduced electron transfer-reversible addition-fragmentation chain transfer (PET-RAFT) polymerization mechanism and the deoxygenation process of g-C_3N_4.[86]

Taking the g-C_3N_4/WO_3 Z-type heterojunction as an example, the electrons in the conduction band of WO_3 combine with the holes in the valence band of g-C_3N_4 under light, and at the same time, the electrons in the conduction band of g-C_3N_4, which have a stronger reducing capacity, and the holes in the valence band of WO_3, which have a stronger oxidizing capacity, are retained, and the system is able to maintain a higher redox capacity at the same time because of the unique charge transfer path.

Electron paramagnetic resonance (EPR) and radical trapping experiments clarified the mechanism of action of different ROS in RhB degradation. It was found that $^{\bullet}OH$ mainly attacked the conjugated chromophores in RhB molecules and triggered the ring-opening reaction, while $^{\bullet}O_2^-$ tended to participate in the de-ethylation process, and the contribution of $^1O_2$ to the degradation of RhB was closely related to its generation. These mechanistic-level insights provide an important basis for the targeted design of efficient g-C_3N_4 photocatalysts. For dye pollutants with azo structures, $^{\bullet}OH$ generation can be enhanced by modulating the energy band structure of the material, whereas for pollutants with benzene ring structures, Z-type heterojunctions can be constructed to increase the yields of $^{\bullet}O_2^-$ and $^{\bullet}OH$ simultaneously.

A study of the photocatalytic degradation mechanism revealed that g-C_3N_4 matrix composites significantly enhanced the catalytic performance through various modification strategies. These modifications not only optimized the charge separation efficiency of the materials but also enhanced the degradation effect by modulating the type and ratio of generated ROS. An in-depth understanding of the constitutive

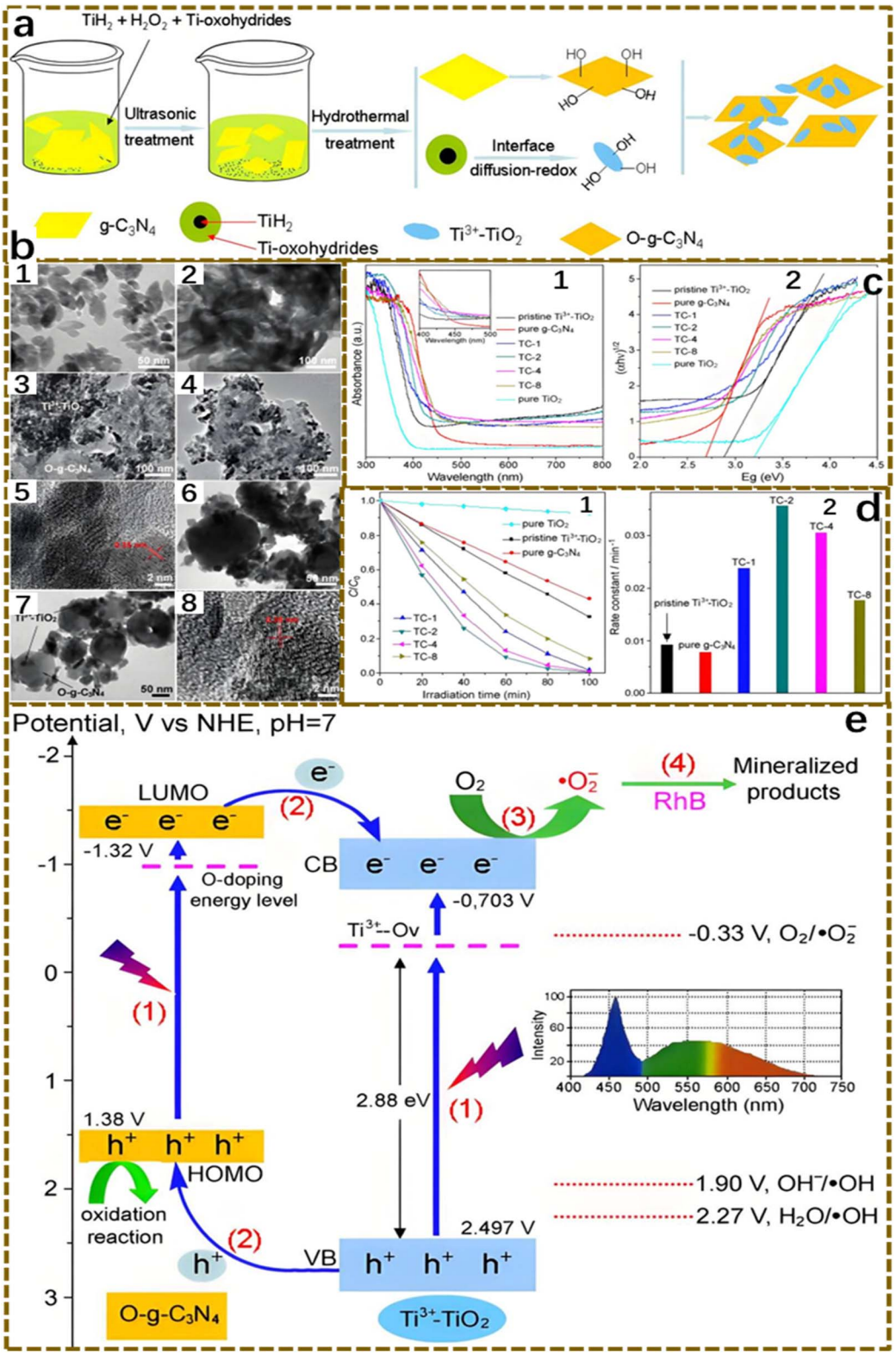

Fig. 9 (a) Sketch of the preparation process for Ti^{3+}-TiO_2/O-g-C_3N_4; (b) TEM and HRTEM images of (1) original Ti^{3+}-TiO_2, (2) pure g-C_3N_4, (3) TC-1, (4,5) TC-2, (6) TC-4, and (7,8) TC-8 samples; (c) (1) UV-DRS of pure g-C_3N_4, TiO_2, Ti^{3+}-TiO_2/O-g-C_3N_4 and Ti^{3+}-TiO_2 heterojunctions; (2) plots of Kubelka–Munk function *versus* photon energy for various samples; (d) (1) rhodamine B photodegradation phenomenon; (2) the degradation rate constants for diverse samples exposed to 30-watt visible-light; (e) schematic diagram of the energy bands of O-g-C_3N_4 and Ti^{3+}-TiO_2 as well as the migration and separation of charges in the O-g-C_3N_4/Ti^{3+}-TiO_2 heterojunction induced by LED illumination.

relationships between interfacial charge transfer mechanisms (type II, Z and S heterojunctions) and ROS generation pathways (including $^{\bullet}O_2^-$, $^{\bullet}OH$ and $^1O_2$) provides important theoretical guidance for the development of efficient g-C_3N_4 photocatalysts with different pollutant properties. Future studies should further combine *in situ* characterization techniques and theoretical calculations to elucidate the precise ROS generation mechanism and their interaction with pollutants under different modification strategies.

4.2. Synergistic effects of composite materials

The combined impact of g-C_3N_4 with other catalysts or cocatalysts during the photocatalytic reaction is also a key factor in improving its photocatalytic performance. For example, combining g-C_3N_4 with noble metals (*e.g.*, Pt, Au, *etc.*) or semiconductor materials (*e.g.*, ZnO, TiO_2, *etc.*) has the capacity to form a heterojunction structure or a Schottky barrier, which facilitates the dissociation and movement of photogenerated electron–hole pairs and enhances the photocatalytic efficiency. This remarkable synergistic effect in the photocatalytic reaction significantly helps to achieve more efficient photocatalytic performance and broader applications. Liu *et al.* chose urea as the precursor and successfully designed and synthesized heterojunction photocatalysts that combine g-C_3N_4 and TiO_2 nanotubes *via* a one-step chemical vapor deposition technique. The comprehensive characterization results clearly show that this composite structure has an excellent cooperative effect on g-C_3N_4 and TiO_2 nanotubes, while well preserving the original structural features of both g-C_3N_4 and TiO_2 nanotubes.[87] In another study, modified g-C_3N_4 doped with lithium and deposited silver was prepared by Ma *et al.* The composite exhibited excellent photocatalytic performance for the degradation of RhB. The introduction of lithium and silver can effectively enhance the light absorption in the visible wavelength rang, impede the combination of photogenerated electron–hole pairs, and enhance the generation of active substances. Owing to the synergistic effect of lithium doping and silver deposition, there was an enhancement in the photocatalytic activity of g-C_3N_4.[88] In 2023, Gomathi *et al.* hydrothermally synthesized CeO_2/Bi_2MoO_6/g-C_3N_4 ternary nanocomposites. Under visible light, these composites achieved a 94% degradation rate within just 100 min, outperforming the original and binary materials. The superior performance stems from the highly efficient carrier migration across the interfaces of CeO_2, Bi_2MoO_6, and g-C_3N_4. Additionally, the material exhibited an expanded light absorption range and a reduced band gap of 2.2 eV (Fig. 9).[77]

The core mechanism of the photocatalytic degradation of RhB by g-C_3N_4 is based on its semiconducting properties. g-C_3N_4 generates photogenerated electron–hole pairs under visible light excitation, and the conduction band electrons (−1.09 eV) reduce dissolved oxygen to generate superoxide radicals ($^{\bullet}O_2^-$), whereas the valence band holes (1.56 eV) oxidize water molecules to generate reactive hydroxyl radicals ($^{\bullet}OH$). These two strongly oxidizing species, gradually degrade RhB through de-ethylation, conjugate structure cleavage and ring opening reactions. The current study aims to analyze the dynamic path and master control mechanism of the synergistic action of multiple radicals, overcome the limitations of the charge transfer efficiency caused by lattice mismatch and defective states at heterojunction interfaces, quantify the interference effects of complex water background components on the radical chain reaction, and solve the cyclic stability attenuation caused by photocorrosion and toxic intermediates. In the future, we should integrate atomic energy band regulation, mesoscopic mass transfer optimization and reaction interface engineering to construct a highly efficient system of "light absorption–charge separation–interface reaction–product desorption" and promote practical environmental applications.

5. Applications of g-C_3N_4-based photocatalytic materials

5.1. Energy utilization

As an inexhaustible natural resource, solar energy is widely regarded as an important pillar of future energy systems with incomparable sustainability and environmental friendliness. In this context, the photocatalytic technology of g-C_3N_4-based composites stands out as an effective way to achieve efficient conversion and utilization of solar energy. As an emerging photocatalyst, g-C_3N_4 shows remarkable light absorption and photoresponsivity within the visible spectrum. This is attributed to its distinctive electronic structure and physicochemical characteristics. *Via* ingenious design and synthesis, g-C_3N_4-based composites are able to fully utilize the visible portion of the solar spectrum to initiate a series of photocatalytic reactions, including water splitting, degradation of organic contaminants, hydrogen generation, and carbon dioxide reduction.[89–94] These reactions not only realize the transformation of solar energy into chemical energy but also offer practical approaches to address global issues like the energy crisis and environmental pollution. During the photocatalytic process, g-C_3N_4-based composites are capable of absorbing visible light and generating photogenerated electrons and holes. These photogenerated carriers separate and move either within the material or on its surface, and this sequential process sets off redox reactions. Through reasonable material design and structural adjustment, the separation efficiency and reactivity of the photogenerated carriers can be remarkably enhanced.[95,96] In addition, g-C_3N_4-based composites have good stability and recyclability and can maintain high activity during long photocatalytic reactions, which reduces the operating cost and environmental risk.[97,98] These features endow g-C_3N_4-based composites with extensive application potential in solar energy conversion and utilization scenarios. In their research, Bian and colleagues employed chemical vapor codeposition to fabricate Cu/Fe bimetallic-modified g-C_3N_4 sheets on carbonized teak peel (Cu/Fe–CNC) for photocatalytic reduction of CO_2 to CO. The performance of Cu/Fe–CNC was three times better than that of bulk g-C_3N_4 and twice that of g-C_3N_4 on CNCs. Moreover, it could attain a 100% conversion rate from CO_2 to CO. Cu/Fe–CNC remained stable for 5 cycles, providing a new method for CO_2 reduction.[99]

5.2. Materials science

Research centered on the meticulous preparation and strategic alteration of g-C_3N_4- based composites is undoubtedly a significant and far-reaching breakthrough in the dynamic field of materials science. It not only remarkably deepens our in-depth understanding of this advanced material but also innovatively opens up a brand-new path for the development of novel and highly efficient photocatalysts. Through fine chemical synthesis and structural design, researchers have successfully synthesized a set of g-C_3N_4-based assemblies with excellent properties, which show unprecedented activity and stability in the field of photocatalysis. Moreover, surface modification, elemental doping and other modifications of g-C_3N_4 have been reported.[100,101] The capacity to absorb light, the efficiency in separating charges, and the catalytic activity were all further increased, providing valuable strategies and methods for optimizing the performance of photocatalysts.[102–104] Ye and colleagues devised a new type of Zn/Cl-doped hollow microtubular g-C_3N_4 (Zn-HT-CN) through a hydrothermal approach. In this process, melamine and zinc chloride were utilized as raw materials. Compared with pure g-C_3N_4 microtubes, Zn-HT-CN managed to achieve a 94.41% photodegradation rate. The photodegradation of tetracycline hydrochloride (TCH) was achieved under visible light irradiation within 40 minutes. This degradation rate was approximately twice that of pure g-C_3N_4 microtubes, showing a significant improvement. Moreover, the performance of Zn-HT-CN was superior to that of g-C_3N_4 microtubes doped with other typical metal elements. In addition, Zn-HT-CN showed good tolerance to environmental pH, and after completing five cycles, the catalytic efficiency of the material remained stable at 78.78%.[105] Liu *et al.* prepared a Z-type heterojunction material, TBCN, by loading Ti MOFs onto two-dimensional g-C_3N_4 nanosheet structures (BCNs) doped with B atoms *via* calcination. Under visible light, the rate of hydrogen generation by TBCN under photocatalytic conditions reached 1242 μmol h^{-1} g^{-1}. This rate is 2.2 times greater than that of BCN and 9.34 times higher compared to the blocks. Experimental findings regarding graphitic carbon nitride (GCN) revealed that the fabrication of Z-type heterojunction composites (TBCNs) could efficiently regulate the position of the material's band gap. This construction expanded the scope of light absorption, promoted electron transfer, and suppressed electron–hole recombination. These effects are essential for achieving high-efficiency photocatalysis.[106] These research findings have not only augmented the theoretical framework of materials science but also provided robust technical support for addressing global issues like the energy crisis and environmental pollution. This suggests that photocatalytic technology is set to assume an even more crucial part in future sustainable development scenarios.

5.3. Industrial application

Photocatalytic technology based on g-C_3N_4 matrix composites, due to their unique advantages of high efficiency and environmental protection, has shown extremely broad application prospects. In heavy pollution industries such as printing and dyeing, papermaking and textiles,[107–109] this technology can efficiently degrade organic pollutants in wastewater, such as dyes, auxiliaries and fiber fragments, significantly improving the efficiency and quality of wastewater treatment. In addition, the photocatalytic technology of g-C_3N_4 matrix composites can serve as a useful reference for the treatment of other types of organic pollutants. For organic wastewater from chemical production, pesticide residues in agriculture,[110] and even organics that are difficult to degrade in municipal wastewater,[111,112] this technology has the potential to achieve the goal of efficient and green treatment through further optimization and innovation. Tang *et al.* directly calcined melamine-loaded TiO_2 nanotube arrays (TNTAs) to produce g-C_3N_4/TiO_2 nanotube array (TCN) photoelectrodes. The TCN photoelectrodes exhibited outstanding photoelectrocatalytic (PEC) capabilities for degrading organic pollutants. In the continuous-flow PEC process without a background electrolyte, 80% of tetracycline was removed from real effluent. Moreover, the TCN photoelectrodes maintained stable performance even after 20 hours.[113] The wide application of these technologies can help solve current serious environmental pollution problems.

5.4. Environmental protection

5.4.1. Degradation of RhB by g-C_3N_4-based composites. RhB, a common hazardous dye in wastewater, poses a substantial risk to the environment and the health of human beings because of its strong carcinogenicity and resistance to natural degradation. However, with the advancements in science and technology, the highly efficient photocatalytic degradation technology of graphite-phase carbon nitride-based composites provides a new way to solve this problem. This technology makes use of the powerful catalytic effect of graphite-phase carbon nitride matrix composites under light conditions, which can rapidly decompose dye molecules, such as RhB, into harmless small molecules, such as water and carbon dioxide, thus realizing a green and environmentally friendly treatment of dye wastewater.[114,115] The successful application of this technology not only effectively reduces the pollution of dye wastewater in the environment but also provides valuable experience and insights for the removal of other hazardous substances. As the technology of graphite-phase carbon nitride-based composites continues to mature and be optimized, the photocatalytic degradation by these composites is predicted to hold an increasingly vital place. In the coming days, with the further development and refinement of this technology, the photocatalytic degradation of graphite-phase carbon nitride-based composites is likely to play a more significant role in environmental protection. Divya Janardhana and colleagues synthesized Bi_2O_3:1 mol%Eu^{3+}/x wt% g-C_3N_4 (where $x = 1$, 3, 5 and 7) composites. The catalytic degradation of RhB in aqueous solution revealed that the 7 wt% g-C_3N_4-modified Bi_2O_3:1 mol% Eu^{3+} product exhibited optimum activity, which was demonstrated under UV-visible light, attaining a maximum dye degradation rate of 98%.[116] Pandey *et al.* prepared LBG-*s*-AgNP@g-C_3N_4NS hybrid nanocomposites by anchoring AgNPs to g-C_3N_4. Under visible light irradiation, the material

demonstrated remarkable performance. It degraded nearly 100% of RhB and around 99% of MB within 160 minutes. This indicates its high efficiency in quickly eliminating harmful dyes. Moreover, the material exhibits notable antibacterial activity against both Gram-positive and Gram-negative bacteria.[117] The material was also found to be effective in degrading harmful dyes. Li *et al.* prepared a single class of algal g-C_3N_4 photocatalytic multifunctional separation membranes by vacuum self-assembly, which exhibited good degradation of eight pollutants, with RhB degradation rates of nearly 100% and antimicrobial efficiencies (*E. coli* and *S. aureus*) of nearly 100%. The membrane performance remained excellent after 35 cycles of C/W emulsion separation and 10 cycles of RhB degradation.[118]

5.4.2. Degradation of methylene blue by g-C_3N_4 matrix composites. Methylene blue (MB), an organic dye, has demonstrated wide applications in several industries. Not only does it play an important role in providing color in traditional manufacturing industries, such as textiles, printing and dyeing, leather, rubber and plastics, but it also has antibacterial, antiviral and antitumour properties, making it valuable as a disinfectant and oxidizing agent in the pharmaceutical field. However, MB is often released in natural water sources posing hazards to human and microbial health.[119] Liu *et al.* constructed a complex system for photocatalytic and advanced oxidation processes by combining g-C_3N_4 with hydrogen peroxide (H_2O_2) to achieve a degradation rate of approximately 94.2% in 50 min with MB as the target pollutant.[120] Solayman *et al.* modified block g-C_3N_4 by acid stripping in a study in which sulfuric acid-treated g-C_3N_4 photocatalysts (CN–S) degraded approximately 93.12% of MB within 150 minutes under unobstructed sunlight, and the degradation performance of MB dyes decreased by only 4.8% in five cycles, demonstrating excellent recyclability.[121] Cao *et al.* prepared g-C_3N_4@$Co_3V_2O_8$ Z-type heterojunction photocatalysts *via* hydrothermal and wet impregnation treatments. The g-C_3N_4@$Co_3V_2O_8$ composite, incorporating 10% g-C_3N_4, exhibited significantly improved photocatalytic degradation capabilities. It achieved a 93.7% removal rate of methylene blue (MB) in aqueous solution within 60 minutes under visible light irradiation. This performance surpassed that of pure $Co_3V_2O_8$ and g-C_3N_4 by 3.1-fold and 1.9-fold, respectively, highlighting the synergistic effect of the composite structure in enhancing photocatalytic activity. The results suggest that the integration of g-C_3N_4 with $Co_3V_2O_8$ effectively promotes charge separation and light absorption, leading to superior degradation efficiency of organic pollutants in water treatment application.[122] Using $CaCO_3$ microspheres as templates, Wang *et al.* synthesized g-C_3N_4 hollow microspheres, achieving a photodegradation efficiency of ~94.3% within 1 hour for MB solutions with concentrations up to 160 mg L^{-1}, attributed to enhanced light

Table 3 Visible-light-driven applications of various g-C_3N_4 composites

Materials	Synthesis method used	Photocatalyst dosage	RhB concentration	Light source power	Degradation time	Photodegradation	Ref.
$CoFe_2O_4$/PDA/g-C_3N_4	Deposition method	1 g L^{-1}	10 mg L^{-1}	12 W	60 min	99.85%	Patra[130]
CFc/g-C_3N_4	Dip-coating and following a pyrolysis method	50 ± 20 mg			80 min	94.8%	Zhu[131]
BiOBr/g-C_3N_4/$Ti_3C_2T_x$	*In situ* construction method	5 mL	10 mg L^{-1}	Xenon lamp below 500 W	50 min	98%	Wu[132]
cPTA/CNT/CNU		30 mg	10 mg/mL	500 W	60 min	95%	Wang[133]
ZrO_2(25%)/g-C_3N_4	Hydrothermal methods	20 mg	10 mg/mL	250 W	120 min	99.5%	Kumari[134]
g-C_3N_4	Thermal condensation technique	0.2 g	50 mg L^{-1}	300 W		95%	Kumar[135]
g-C_3N_4[U]/ZnO		15 mg	10 mg L^{-1}	50 W	60 min	82%	Gotipamul[136]
g-C_3N_4/α-Bi_2O_3/MWCNT	Wet impregnation technique	0.1 g		500 W		93.53%	Palanisamy[137]
MoS_2@MoO_3/(Cu^+/g-C_3N_4)	Calcination method	0.1 g L^{-1}	10 mg L^{-1}	2.96 eV	40 min	99.41%	Hong[138]
ZnO/Ag/g-C_3N_4	One-step polymer-network gel method	50 mg	8 mg L^{-1}	50 W	30 min	100%	Li[139]
2D/3D CNSCN		10 mg		300 W	80 min	100%	Xing[140]
Lignin@t-FeC_2O_4/g-C_3N_4	Impregnation coating and precipitation reaction		30 mg L^{-1}	200 W	40 min	90%	Xiong[141]
g-C_3N_4	One-pot cosolvothermal method	30 mg	200 mg L^{-1}	1000 W		98.8%	Huang[142]
P–UCN1/S-TCN1	Copolymerization		5 mg	50 W	30 min	100%	Wu[143]
CDs@CN		0.1–5.0 wt%	20 mg L^{-1}		60 min	95%	Li[144]
KPCN/GO/$ZnFe_2O_4$	Hydrothermal method	0.6 g L^{-1}	9.85 mg L^{-1}	500 W	60 min	87%	Kumar[145]
ACB-K-g-CN	Innovative ultrasonic-milling method	1 g L^{-1}	200 mg	500 W		93.26%	Wang[146]
g-C_3N_4 nanosheet/$CuBi_2O_4$/Bi_3ClO_4		100 mg	5 mg	50 W	20 min	98%	Mousavi[147]
g-C_3N_4	Environmentally friendly chemical and thermal methods	10 mg	10 mg L^{-1}	300 W	60 min	93.5%	Amiri[148]

absorption and active site.[123] Chen *et al.* prepared a novel MgAlTi-LDH/g-C_3N_4 heterojunction, which achieved a 95% degradation rate of MB within 130 minutes under natural sunlight irradiation.[124] The results of these experiments provide insights for the removal of MB from wastewater. In order to further demonstrate the performance of various types of g-C_3N_4 composites under visible light-driven conditions, the relevant content is organised in Table 3.

5.4.3. Malachite green degradation using g-C_3N_4 composites. Malachite green (MG), a toxic triphenylmethane compound, is widely used as a parasitic agent in aquaculture to control fish parasites and water molds. It is also used as a preservative in the food and textile industries for dyeing materials such as nylon, wool and silk. However, MG is highly toxic and carcinogenic, and its degradation is also a major challenge in environmental remediation. Thangavelu *et al.* synthesized $ZnBi_2O_4$/g-C_3N_4 p–n heterojunction nanocomposites, which showed the highest degradation efficiency of 90% for MG within 100 min under visible light illumination.[125] Merci *et al.* prepared g-C_3N_4/Bi_2S_3/$NiFe_2O_4$ nanocomposites with a double Z-type heterojunction, which resulted in 95.63% photocatalytic degradation of MG under optimum conditions. The photodegradation rate constant of MG on g-C_3N_4/Bi_2S_3/$NiFe_2O_4$ was 0.0504 min^{-1}, and the prepared catalysts were found to be stable after six cycles of photocatalysis.[126] Sudha *et al.* prepared (ZnO : Ce)green/g-C_3N_4, which achieved 99% detoxification efficiency for MG. The material also exhibited significant antioxidant, antidiabetic and anti-inflammatory activities, with inhibition percentages of 87, 92 and 90%, respectively.[127] Bibi *et al.* prepared Gd1-xSmxFeO$_3$@g-C_3N_4 nanocomposites with a spiky circular spherical structure, achieving 93% degradation of MG.[128] These findings show that g-C_3N_4 has great potential as an environmentally friendly photocatalyst. Its unique properties effectively promote the photocatalytic reaction for efficient degradation of industrial dye wastes while showing promising applications for the treatment of potential biomedical reagents (Fig. 10).

The g-C_3N_4-based composites show significant advantages in the field of photocatalytic degradation due to their excellent visible light responsiveness, good chemical stability and recyclability. However, the technology still faces key challenges. The specific surface area, light absorption range and carrier

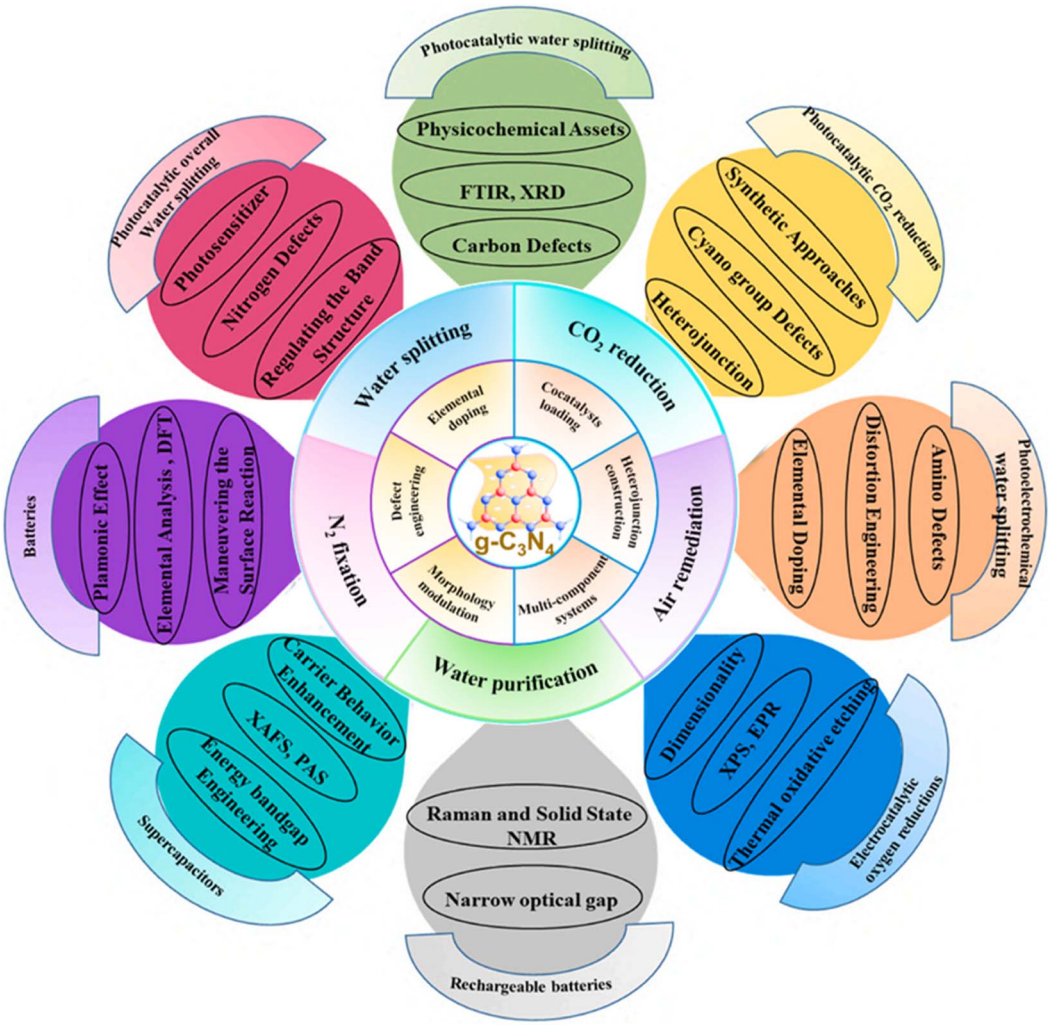

Fig. 10 Utilization of g-C_3N_4 composites.[21,129]

complexity of pristine materials need to be optimized; the complexity and reproducibility challenges of the scale-up preparation process of composites need to be overcome; and catalyst recyclability, long-term cycling stability and adaptability to complex aqueous environments need to be improved for practical applications. In addition, the utilization rate of the full spectrum of sunlight (especially near-infrared light) still needs to be improved. Future research should focus on optimizing the structural properties of the materials, modulating the photo-generated charge dynamics and increasing their suitability for practical applications to achieve more efficient and stable environmental treatment applications (Fig. 11).

5.4.4. Degradation of antibiotics by g-C_3N_4-based composites. g-C_3N_4-based composites have shown remarkable results in the photocatalytic degradation of dyes, achieving efficient removal of dyes through various composite strategies. However, the diversity of environmental pollutants requires further research. With the extensive use of antibiotics in the medical and aquaculture industries, the problem of their residual pollution is becoming increasingly prominent, and the complex structure and high stability of antibiotics make them difficult to degrade completely *via* traditional treatment methods. Owing to the excellent photocatalytic performance and mechanism of action of g-C_3N_4 matrix composites in dye

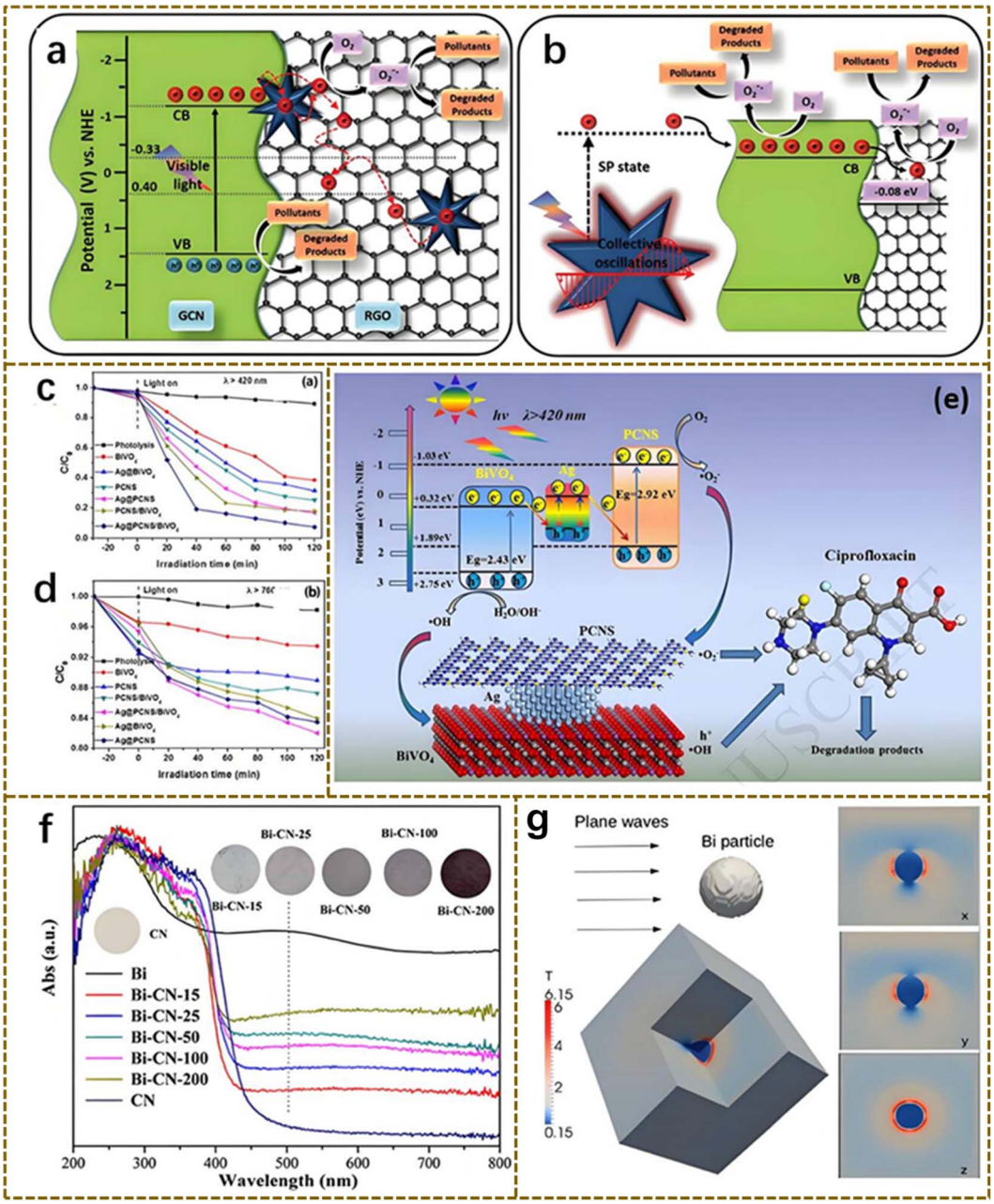

Fig. 11 (a and b) Proposed mechanism for MB and TC degradation using Au NST-GCN/RGO under visible light. (c and d) CIP degradation performance under visible and NIR light for various samples. (e) Suggested dual Z-scheme mechanism for CIP degradation *via* Ag@PCNS/$BiVO_4$. (f) UV-Vis DRS spectrum with sample images (inset) and (g) SPR-induced electromagnetic field in Bi metal.[149]

degradation, their application in antibiotic degradation has become a highly promising research direction.

To overcome the inherent limitations of pristine g-C_3N_4, such as fast charge complexation and limited visible light absorption, the composites were engineered through strategies such as heterojunction formation, elemental doping, coupling with carbon materials or doping with metal nanoparticles. Liu *et al.* prepared S-deficient $Bi_4O_5I_2$/CN S-scheme heterojunction composites *via* a solvothermal method. Under visible light, the optimized S–$Bi_4O_5I_2$/CN (10%) demonstrated significantly superior photocatalytic activity compared with $Bi_4O_5I_2$, achieving complete degradation of 50 mg L^{-1} tetracycline hydrochloride (TC) within just 10 minutes. The material exhibits broad applicability, effectively degrading various tetracycline antibiotics while maintaining high efficiency at different pollutant concentrations and pH levels.[150] Lin *et al.* fabricated visible light-driven MX@MCN nanocomposites *via* a solvothermal method. The material exhibited a reduced band gap (from 2.7 eV to 2.4 eV) and an extended photon lifetime (from 4 ns to 6 ns) due to the formation of an indirect Z-scheme heterojunction. It achieved nearly complete removal (>99%) of 10 mg L^{-1} enrofloxacin (ENR) under visible light irradiation.[151] Wang *et al.* prepared porous g-C_3N_4 nanosheets (UCNs) *via* the thermal polymerization of urea. The UCN550 sample exhibited excellent photocatalytic activity under both visible light and sunlight, removing >94% of the tetracyclines (TCs) from the biogas slurry after just 30 minutes of solar irradiation. Comparative studies demonstrated that UCN550-1 shows promising performance in degrading antibiotics in real wastewater, with high potential in terms of synthesis simplicity, efficiency, cost-effectiveness, and engineering applicability.[152]

The g-C_3N_4 matrix composites have great potential for application in antibiotic contamination treatments because of their accumulated photocatalytic advantages in dye degradation. To overcome the shortcomings of the original g-C_3N_4, such as fast charge complexation and limited visible light absorption, the photocatalytic degradation performance of a variety of antibiotics, such as tetracyclines and fluoroquinolones, has been significantly improved by the optimization of heterostructure construction and elemental doping strategies, providing a highly efficient and promising solution with engineering applications for solving the problem of residual antibiotic contamination.

6. Conclusions and prospects

6.1. Conclusion

With its strong visible-light absorption capability, g-C_3N_4 has emerged as a highly efficient photocatalyst, demonstrating significant potential in the photocatalytic degradation of organic dyes. Particularly, it excels in degrading RhB, a dye associated with substantial ecological and health risks, making it a promising material for environmental remediation and sustainable water treatment applications. In this paper, we review recent studies on the enhancement of photocatalytic efficacy through surface functionalization and morphological engineering and analyze multiple crucial elements that have an impact on the performance of g-C_3N_4 during the catalytic degradation process of RhB. We summarize the functions of reactive oxygen species generation and interfacial charge transfer pathways in boosting the efficiency of the g-C_3N_4 photocatalytic system. Also included are the impacts of repeated recycling on the performance of g-C_3N_4-based photocatalytic materials, inter-component interactions affecting their overall photocatalytic performance, and the application directions of composites centered around g-C_3N_4. These significant findings clearly reveal the great and broad potential of g-C_3N_4 as an efficient photocatalyst in diverse applications, such as environmental purification and renewable energy conversion. They not only provide theoretical support for the modification design of g-C_3N_4 but also lay a solid foundation for promoting its application expansion in environmental purification and other fields.

6.2. Challenges ahead

6.2.1 Photocatalytic efficiency enhancement. The band gap of g-C_3N_4 is wide (approximately 2.7 eV), and g-C_3N_4 absorbs mainly UV light and some visible light, with a limited light absorption range and low utilization of sunlight, limiting its photocatalytic performance. The photogenerated electron–hole pairs are prone to rapid complexation, leading to a reduction in the number of effective carriers and lowering the effectiveness of the photocatalytic reaction. The small specific surface area and the relatively limited number of active sites in bulk g-C_3N_4 severely affect the adsorption of reactants and the catalytic activity of the material. g-C_3N_4 has low electrical conductivity, which limits the photogenerated electron transport efficiency and further affects the catalytic performance. Under prolonged light exposure or harsh reaction conditions, g-C_3N_4 may undergo photocorrosion or structural degradation, affecting its durability.

6.2.2 Adaptability to complex water conditions. g-C_3N_4 has excellent photocatalytic degradation performance under laboratory conditions, but in practical applications, the absorptive efficiency of visible-light still needs to be improved, the electron–hole complex problem needs to be continuously optimized, and the interference problem of coexisting pollutants in the environment on the performance of the catalysts has not yet been completely solved, requiring the development of g-C_3N_4 heterojunctions with interference resistance to increase their adaptability in real wastewater treatment.

6.2.3 Difficulties in scale-up preparation. The preparation process of nanostructures (*e.g.*, nanosheets and porous structures) or composites optimized in the laboratory is complicated and difficult to scale up directly to industrial production. The manufacturing of high-quality g-C_3N_4 usually requires high-temperature and long-term heat treatment, which is energy intensive and costly, making it difficult to meet the economic requirements for large-scale production. The purity and consistency of raw materials in large-scale production are highly important, and impurities or batch differences may affect the stability of material properties. Moreover, existing laboratory equipment has difficulty meeting the needs of large-scale

continuous production, and it is necessary to develop suitable industrial-grade reactors and production processes. Ensuring the consistency and controllability of material properties (*e.g.*, specific surface area, photoabsorption, and catalytic activity) during the large-scale preparation process is a major challenge. Large-scale production may involve high temperatures, high pressures or hazardous chemicals, and environmental and safety issues need to be addressed.

6.2.4 Synergistic optimization of environmental factors. The presence of multiple pollutants (*e.g.*, organic matter, heavy metals, and microorganisms) in the actual environment and the need for g-C_3N_4 to achieve both efficient degradation and stability under complex conditions necessitate increased requirements for material design. g-C_3N_4 heterojunctions are significantly affected by the instability of environmental conditions, for example, pH, temperature, light intensity, dissolved oxygen, pollutant concentration, and coexisting ions, which have a significant impact on the photocatalytic performance of the heterojunctions, and it is necessary to achieve synergistic interactions between environmental conditions and catalytic performance through the modulation of environmental factors. It is necessary to improve degradation efficiency by regulating environmental factors and optimizing the heterojunction structure to achieve a synergistic effect between environmental conditions and catalytic performance. Moreover, the photocatalytic degradation process may produce toxic intermediate products or secondary pollution, and the reaction path should be optimized to reduce harmful byproducts. In complex environments, g-C_3N_4 may be deactivated by photocorrosion, chemical erosion or mechanical abrasion, affecting long-term stability, and its durability and reusability need to be improved.

6.3. Directions for development

6.3.1 Material optimization. The development of more efficient multifunctional composites that combine doping, heterostructure building and surface modification can maximize photocatalytic performance. The specific surface area and the number of active sites can be increased by the production of nanosheets, nanotubes or porous structures to increase light absorption and catalytic activity. Sophisticated doping strategies, like B, P, and S doping or Fe, Co, and Ni doping, and elaborate composite structure constructions, such as composites with TiO_2, MoS_2 or carbon materials, are skillfully utilized to delicately modulate the energy band structure and prominently enhance the carrier separation efficiency and electrical conductivity. Defects or functional groups are introduced into surface modifications and energy band engineering to further optimize light absorption and reactivity. More precise interfacial modulation techniques have been investigated to increase the charge separation efficiency and photocatalytic stability.

6.3.2 Applications under practical conditions. Since g-C_3N_4 is a photocatalyst that responds to visible light, it has potential for application in the solar-driven hydrogen generation process through the decomposition of water, providing a feasible path for clean energy development. g-C_3N_4-based materials are additionally in a position to achieve the photocatalytic transformation of CO_2 to fuels such as methane and methanol, thus contributing to carbon neutralization and renewable energy conversion. In pollutant degradation, g-C_3N_4 is capable of being employed for the photocatalytic decomposition of organic contaminants (such as dyes and antibiotics) and the elimination of heavy metal ions, which can efficiently enhance water quality. When used as an electrode material, g-C_3N_4 displays excellent electrochemical properties in supercapacitors and lithium-ion batteries, which is conducive to enhancing the energy storage efficiency. The high specific area of the surface and tunable electronic structure of g-C_3N_4 make it potentially valuable for applications in gas sensing and biodetection fields with potential applications. Improving the adaptability of g-C_3N_4 heterojunctions in real environmental pollution treatment for complex environments.

6.3.3 Engineering and scale-up. Low-energy and environmentally friendly synthesis methods, such as low-temperature solid–phase reactions or hydrothermal methods, have been developed to reduce the production cost and reduce environmental pollution. The reaction conditions (*e.g.*, temperature, pressure, and raw material ratio) should be optimized, and continuous production equipment should be designed to achieve efficient, stable and large-scale preparation of g-C_3N_4 materials. The chemical stability and durability of materials in real environments (*e.g.*, high temperature, strong light, acidic and alkaline conditions) can be increased through doping, compositing or surface modification. g-C_3N_4-based materials with multiple functions, such as photocatalysis, electrocatalysis and sensing, have been developed, expanding their application across energy, the environment, industry and other fields. Material performance evaluation standards and production quality control systems should be established to ensure consistent performance and reliability of scaled-up products. Exploring cost-effective scale-up preparation methods is essential to reduce production costs and improve the technical feasibility and market competitiveness of g-C_3N_4-based composites.

6.3.4 Environmental friendliness and economy. Low-energy, nonpolluting preparation methods have been developed to reduce the use of toxic reagents and reduce their impact on the environment. g-C_3N_4 can be synthesized *via* the use of inexpensive and renewable precursors (*e.g.*, urea and melamine) to reduce raw material costs and increase sustainability. The light absorption and catalytic efficiency of a material can be improved through structural modulation (*e.g.*, nanosheets and porous structures) and doping modifications to reduce resource consumption and achieve efficient use of resources. The chemical stability and recyclability of materials should be increased to extend their service life and reduce waste generation. The production process should be optimized to achieve continuous and automated production and reduce the cost of large-scale preparation. g-C_3N_4-based materials with multiple functions, such as photocatalysis, electrocatalysis and sensing, have been developed to expand multifunctional applications and increase their economic value.

Data availability

No primary research results, software or code have been included and no new data were generated or analysed as part of this review.

Author contributions

Meie Zheng and Mengru Guo: Writing–original draft, visualization, project administration, conceptualization. Meie Zheng and Fei Ma: Writing–review & editing, funding acquisition, supervision. Wenwen Li and Yujia Shao: Investigation, formal analysis, methodology, resources.

Conflicts of interest

The authors declare no competing financial interest.

Acknowledgements

This work was supported by the Natural Science Foundation Project of Hubei Province (2022CFB533), the Natural Science Project of Xiaogan city (XGKJ2024030002), Hubei Small Town Development Research Center 2025 Annual Open Research Project (2025K011), College Student Innovation Project Training Program (S202510528048), and Outstanding Course Ideological and Political Education Projects (KCSZ202529).

References

1 C.-S. Chiou, H.-W. Chen and Z.-T. Chen, *Int. J. Environ. Sci. Technol.*, 2018, **15**, 1879–1886.
2 T. Chadelaud, H. Zeghioud, A. Reynoso De La Garza, O. Fuerte, A. Benítez-Rico, M. Revel, T. E. Chávez-Miyauchi and H. Djelal, *Processes*, 2023, **11**, 2671.
3 A. Al Miad, S. P. Saikat, Md. K. Alam, Md. Sahadat Hossain, N. M. Bahadur and S. Ahmed, *Nanoscale Adv.*, 2024, **6**, 4781–4803.
4 A. Sharma, S. Sunny, J. Arulraj and G. Hegde, *Nano Express*, 2024, **5**, 022002.
5 L. Noureen, Q. Wang, M. Humayun, W. A. Shah, Q. Xu and X. Wang, *Environ. Res.*, 2023, **219**, 115084.
6 J. Zhu, Y. Dong, Q. Wang, J. Han, Z. Li, D. Xu, L. Fischer, M. Ulbricht and Z. Ren, *Sci. Total Environ.*, 2024, **957**, 177595.
7 S. He, Z. Hu, C. He, S. Tian, G. Ouyang, Z. Lin and J. Fang, *Angew. Chem., Int. Ed.*, 2025, **64**, e202424827.
8 M. S. Umekar, G. S. Bhusari, T. Bhoyar, V. Devthade, B. P. Kapgate, A. P. Potbhare, R. G. Chaudhary and A. A. Abdala, *Curr. Nanosci.*, 2023, **19**, 148–169.
9 Q. Hu, M. K. Albolkany, C. Liu, T. Zhang, S. Cui, F. Ye and B. Liu, *Desalination*, 2024, **583**, 117650.
10 J. Fang, L. Liu, H. Yang and H. Du, *J. Environ. Chem. Eng.*, 2024, **12**, 114153.
11 P. Hao, Z. Chen, Y. Yan, W. Shi and F. Guo, *Sep. Purif. Technol.*, 2024, **330**, 125302.
12 A. Verma, G. Sharma, T. Wang, A. Kumar, P. Dhiman and A. García-Peñas, *Carbon Lett*, 2025, **35**, 45–73.
13 N. R. Barveen, B. Parasuraman, P.-Y. Wang, C.-W. Zeng, Y.-W. Cheng and P. Thangavelu, *Surf. Interfaces*, 2024, **53**, 105039.
14 J. Wang and S. Wang, *Coord. Chem. Rev.*, 2022, **453**, 214338.
15 M. A. Ahmed, S. A. Mahmoud and A. A. Mohamed, *RSC Adv.*, 2024, **14**, 25629–25662.
16 Z. Zhao, Y. Sun and F. Dong, *Nanoscale*, 2015, **7**, 15–37.
17 D. M. Teter and R. J. Hemley, *Science*, 1996, **271**, 53–55.
18 F. Su, Z. Wang, H. Xie, Y. Zhang, C. Ding and L. Ye, *Catalysts*, 2022, **12**, 1496.
19 R. Li, J. Luan, Y. Zhang, L. Jiang, H. Yan, Q. Chi and Z. Yan, *Renew. Sustain. Energy Rev.*, 2024, **206**, 114863.
20 Z. Afshari, A. Ramazani and H. Teymourinia, *Inorg. Chem. Commun.*, 2025, **172**, 113709.
21 X.-L. Song, L. Chen, L.-J. Gao, J.-T. Ren and Z.-Y. Yuan, *Green Energy Environ.*, 2024, **9**, 166–197.
22 B. Xu, M. B. Ahmed, J. L. Zhou, A. Altaee, G. Xu and M. Wu, *Sci. Total Environ.*, 2018, **633**, 546–559.
23 H. Jiang, Y. Li, D. Wang, X. Hong and B. Liang, *Curr. Org. Chem.*, 2020, **24**, 673–693.
24 A. Alaghmandfard and K. Ghandi, *Nanomaterials*, 2022, **12**, 294.
25 W. Zheng, C. Ye, M. Yu, S. Yang, Y. Xiu, X. He, H. Xue, J. Xia, R. Gao, Z. Yuan and L. Wang, *Adv. Compos. Hybrid Mater.*, 2025, **8**, 61.
26 X. Xiao, Y. Wang, Q. Bo, X. Xu and D. Zhang, *Dalton Trans.*, 2020, **49**, 8041–8050.
27 J. Li, C. Wang, Y. Ma, K. Li and Y. Mei, *RSC Adv.*, 2023, **13**, 13142–13155.
28 S. He, Y. Chen, J. Fang, Y. Liu and Z. Lin, *Chem. Soc. Rev.*, 2025, **54**, 2154–2187.
29 S. Chand and A. Mondal, *Ceram. Int.*, 2023, **49**, 5419–5430.
30 X. Liu, M. Chen and X. Zhang, *Catal. Sci. Technol.*, 2024, **14**, 4036–4044.
31 C. Bian, B. Zhou, F. Mo, X. Liu, P. Sun and X. Dong, *Sep. Purif. Technol.*, 2023, **325**, 124556.
32 K. Yang, T. Liu, D. Xiang, Y. Li and Z. Jin, *Sep. Purif. Technol.*, 2022, **298**, 121564.
33 Z. Lv, X. Cheng, B. Liu, Z. Guo and C. Zhang, *Appl. Surf. Sci.*, 2020, **504**, 144486.
34 B.-W. Sun, H.-J. Li, H. Yu, D.-J. Qian and M. Chen, *Carbon*, 2017, **117**, 1–11.
35 T. Tian, D. Lu, B. Zhao, K. K. Kondamareddy, W. Gu, J. Yang, H. Hao, H. Fan and W. Ho, *J. Alloys Compd.*, 2025, **1010**, 178135.
36 Q. Deng, R. Li, A. Chen, Y. Zhong, X. Yin, Y. Zhang and R. Yang, *Environ. Res.*, 2023, **238**, 117252.
37 D. Wang, X. Huang, Y. Huang, X. Yu, Y. Lei, X. Dong and Z. Su, *Colloids Surf., A*, 2021, **611**, 125780.
38 J. Ding, Y. Lou, G. Dong and Y. Zhang, *J. Photochem. Photobiol., A*, 2023, **439**, 114590.
39 I. Papailias, N. Todorova, T. Giannakopoulou, N. Ioannidis, P. Dallas, D. Dimotikali and C. Trapalis, *Appl. Catal., B*, 2020, **268**, 118733.

40 Y.-P. Zhu, T.-Z. Ren and Z.-Y. Yuan, *ACS Appl. Mater. Interfaces*, 2015, **7**, 16850–16856.
41 S. Eswaran Panchu, S. Sekar, S. John, S. J. Panchu, T. A. Kumaravelu, H. C. Swart, M. Babu Sridharan, S. Singh, C. Dong and N. Kalkura Subbaraya, *Nanoscale*, 2025, DOI: 10.1039/D5NR01035G.
42 G. Yu, K. Gong, C. Xing, L. Hu, H. Huang, L. Gao, D. Wang and X. Li, *Chem. Eng. J.*, 2023, **461**, 142140.
43 C. Zhang, Q. Wan, H. Yu, J. Li, H. Zeng, H. Pang, W. Zhang, S. Liu, J. Huang and X. Li, *Sep. Purif. Technol.*, 2025, **361**, 131291.
44 X. Xiao, Y. Wang, H. Zhang, Z. Chou, H. Ding, X. Lu, Y. Zou, L. Chen and D. Sun, *J. Alloys Compd.*, 2025, **1022**, 179835.
45 Y. Du, K. Nie, W. Wang, N. Sa, R. Yang, M. Wu, H.-Q. Wang and J. Kang, *Appl. Phys. Lett.*, 2024, **124**, 222101.
46 Y. Shen, J. Shi, Y. Wang, Y. Shi, P. Shan, S. Zhang, J. Hou, F. Guo, C. Li and W. Shi, *Chem. Eng. J.*, 2024, **498**, 155774.
47 A. Khampuanbut, S. Kheawhom, W. Kao-ian, W. Limphirat, H. Uyama and P. Pattananuwat, *J. Power Sources*, 2024, **612**, 234795.
48 Z. Karimzadeh and Z. Shariatinia, *Surf. Interfaces*, 2024, **55**, 105367.
49 M. Afkari, S. M. Masoudpanah, M. Hasheminiasari and S. Alamolhoda, *Sci. Rep.*, 2023, **13**, 6203.
50 S. Sharafinia, A. Farrokhnia, E. G. Lemraski and A. Rashidi, *Sci. Rep.*, 2023, **13**, 21323.
51 Y. Chen, L. Tan, H. Zhang, X. Zhang, Q. Chen, H. Jiang, F. Ge, S. Wei, X. Gao and P. Wang, *Res. Chem. Intermed.*, 2021, **47**, 3349–3362.
52 J. Luo, Z. Dai, M. Feng, M. Gu and Y. Xie, *Nano Res.*, 2023, **16**, 371–376.
53 S. V. P. Vattikuti, N. D. Nam and J. Shim, *Ceram. Int.*, 2020, **46**, 18287–18296.
54 S. Dharani, L. Gnanasekaran, S. Arunachalam, A. Zielińska-Jure, H. S. Almoallim and M. Soto-Moscoso, *Environ. Res.*, 2024, **258**, 119484.
55 S. A. Ghourichay, S. Agbolaghi, R. Corpino and P. C. Ricci, *Molecules*, 2024, **29**, 5439.
56 K. H. Nasir and H. A. Alshamsi, *J. Inorg. Organomet. Polym. Mater.*, 2024, **34**, 5925–5942.
57 M. Yang, X. Li, R. Zhao, Y. Wang, N. Liu, Y. Liu and J. Yang, *CrystEngComm*, 2024, **26**, 5867–5876.
58 J. Shi, T. Chen, C. Guo, Z. Liu, S. Feng, Y. Li and J. Hu, *Colloids Surf., A*, 2019, **580**, 123701.
59 T. M. O. Le, T. H. Lam, T. N. Pham, T. C. Ngo, N. D. Lai, D. B. Do and V. M. Nguyen, *Polymers*, 2018, **10**, 633.
60 J. Yan, Z. Song, X. Wang, Y. Xu, W. Pu, H. Xu, S. Yuan and H. Li, *Appl. Surf. Sci.*, 2019, **466**, 70–77.
61 C. Hong, J. Zhou, W. Wang, L. Wu, S. Long, W. Zhou and Y. Guo, *J. Water Process Eng.*, 2024, **68**, 106384.
62 H. Kong, H. Li, H. Wang, S. Li, B. Lu, J. Zhao and Q. Cai, *Appl. Surf. Sci.*, 2023, **610**, 155544.
63 A. Masoud, M. A. Ahmed, F. Kühn and G. Bassioni, *Heliyon*, 2023, **9**, e22342.
64 Y. Yang, J. Yan, Y. Zhang, S. Xing, J. Ran, Y. Ma and X. Li, *Int. J. Hydrog. Energy*, 2024, **51**, 962–974.
65 Y. Xu, H. Xu, L. Wang, J. Yan, H. Li, Y. Song, L. Huang and G. Cai, *Dalton Trans.*, 2013, **42**, 7604.
66 Y. Li, H. Zhang, P. Liu, D. Wang, Y. Li and H. Zhao, *Small*, 2013, **9**, 3336–3344.
67 X. Zhan, H. Wang, G. Zhou, L. Chen, Y. Sun, Y. Zhao, J. Liu and H. Shi, *ACS Appl. Mater. Interfaces*, 2021, **13**, 12118–12130.
68 Z. Li, Q. Chen, Q. Lin, Y. Chen, X. Liao, H. Yu and C. Yu, *J. Taiwan Inst. Chem. Eng.*, 2020, **114**, 249–262.
69 S. Ji, Y. Yang, Z. Zhou, X. Li and Y. Liu, *J. Water Process Eng.*, 2021, **40**, 101804.
70 J. Qu, Y. Du, Y. Feng, J. Wang, B. He, M. Du, Y. Liu and N. Jiang, *Mater. Sci. Semicond. Process.*, 2020, **112**, 105023.
71 K.-L. Wang, Y. Li, T. Sun, F. Mao, J.-K. Wu and B. Xue, *Appl. Surf. Sci.*, 2019, **476**, 741–748.
72 R. Fatima and J.-O. Kim, *Environ. Res.*, 2022, **205**, 112422.
73 Z. Mohammadi, H. Abbasi-Asl, M. M. Sabzehmeidani, M. Ghaedi and Z. Moradi, *Appl. Clay Sci.*, 2023, **246**, 107182.
74 A. Vadivu, M. Venkatachalam and A. Silambarasan, *Transit. Met. Chem.*, 2025, **2**(0340–4285), 1572–901X.
75 A. Alsulmi, I. A. Hussein, M. Nasherty, M. Hesham, A. Soltan, M. F. A. Messih and M. A. Ahmed, *J. Inorg. Organomet. Polym. Mater.*, 2024, **34**, 640–654.
76 Z. Moghimifar, F. Yazdani, K. Tabar-Heydar and M. Sadeghi, *Catal. Lett.*, 2024, **154**, 1255–1269.
77 A. Gomathi, K. A. Ramesh Kumar and P. Maadeswaran, *Environ. Sci. Pollut. Res.*, 2024, **31**, 48103–48121.
78 M. A. Khan, S. Mutahir, I. Shaheen, Y. Qunhui, M. Bououdina and M. Humayun, *Coord. Chem. Rev.*, 2025, **522**, 216227.
79 M. Zhang, M. Xing, B. Dong, H. Zhang, X. Sun, Q. Li, X. Lu, J. Mo and H. Zhu, *Water*, 2023, **15**, 2903.
80 P. Rohilla, B. Pal and R. K. Das, *Heliyon*, 2023, **9**, e21900.
81 M. Xu, J. Yang, C. Sun, Y. Cui, L. Liu, H. Zhao and B. Liang, *J. Mater. Sci.*, 2021, **56**, 1328–1346.
82 X. Zhang, C. Li, L. Dai, C. Si, Z. Shen, Z. Qiu and J. Wang, *J. Environ. Chem. Eng.*, 2023, **11**, 110869.
83 S. Patnaik, S. Martha, S. Acharya and K. M. Parida, *Inorg. Chem. Front.*, 2016, **3**, 336–347.
84 Q. Liang, J. Jin, C. Liu, S. Xu, C. Yao, Z. Chen and Z. Li, *J. Mater. Sci. Mater. Electron.*, 2017, **28**, 11279–11283.
85 D. Huang, X. Yan, M. Yan, G. Zeng, C. Zhou, J. Wan, M. Cheng and W. Xue, *ACS Appl. Mater. Interfaces*, 2018, **10**, 21035–21055.
86 Q. Cao, B. Kumru, M. Antonietti and B. V. K. J. Schmidt, *Mater. Horiz.*, 2020, **7**, 762–786.
87 R. Liu, Y. Bie, Y. Qiao, T. Liu and Y. Song, *Mater. Lett.*, 2019, **251**, 126–130.
88 W. Ma, X. Wang, F. Zhang, X. Fei, X. Zhang, H. Ma and X. Dong, *Mater. Res. Bull.*, 2017, **86**, 72–79.
89 K. Zhang, R. Wang and F. Jiang, *ACS Omega*, 2023, **8**, 18090–18105.
90 Q. Jian, Z. Jin, H. Wang, G. Wang and Y. Zhang, *J. Sol-Gel Sci. Technol.*, 2019, **90**, 565–577.
91 P. Saini, K. Ahmadizamani, N. Chakinala, S. Mukherjee, G. Sethia, A. Gupta Chakinala and P. K. Surolia, *J. Mol. Struct.*, 2025, **1321**, 140013.

92 L. Dong, Y. Xu, D. Zhong, N. Zhong, Z. Han, Y. Liu and H. Chang, *New J. Chem.*, 2023, **47**, 14828–14839.
93 X. Jing, X. Mi, W. Lu, N. Lu, S. Du, G. Wang and Z. Zhang, *Chin. J. Catal.*, 2024, **67**, 112–123.
94 M. Sun, C. Zhu, S. Wei, L. Chen, H. Ji, T. Su and Z. Qin, *Materials*, 2023, **16**, 6665.
95 S. Wang, H. Yin, L. Wang, J. Ding, J. Zhang, H. Wan and G. Guan, *Nanotechnology*, 2024, **35**, 195605.
96 Y. Zhang, G. Wu, Y. Chen, P. Yan, L. Xu, J. Qian, F. Chen, Y. Yan and H. Li, *J. Environ. Chem. Eng.*, 2023, **11**, 110173.
97 L. S. Alqarni, M. D. Alghamdi, H. Alhussain, N. Y. Elamin, K. K. Taha and A. Modwi, *J. Mater. Sci. Mater. Electron.*, 2024, **35**, 239.
98 X.-J. Lu, L. Xu, I. Ullah, H.-B. Li and A.-W. Xu, *Catal. Sci. Technol.*, 2024, **14**, 606–614.
99 S. Bian, X. Li, L. Zhang, L. Wang, J. Wang, Q. Xu, L. Zang, Y. Zhang and L. Sun, *J. Environ. Chem. Eng.*, 2023, **11**, 109319.
100 Y. Li, T. Zhang, Y. Liu, C. Liu, J. Sun, J. Che, P. Xiong and J. Zhu, *J. Mater. Chem. C*, 2024, **12**, 15934–15945.
101 Z. Sun, Y. Qi, K. Wang, J. Li, X. Qiu, Y. Zhao and L. Guo, *J. Alloys Compd.*, 2024, **1008**, 176712.
102 A. Sherryna, M. Tahir and Z. Y. Zakaria, *Int. J. Hydrog. Energy*, 2024, **51**, 1511–1531.
103 Y. Liu, X. Chen, M. Kamali, B. Rossi, L. Appels and R. Dewil, *Adv. Funct. Mater.*, 2024, **34**, 2405741.
104 S. B. Sundararaj, H. Amir, V. Chinnusamy and S. Thangavelu, *Int. J. Hydrog. Energy*, 2023, **48**, 26221–26237.
105 X.-Y. Ye, Y.-L. Qi, Y. Cheng, Q. Wang and G.-Z. Han, *Langmuir*, 2025, **41**, 1684–1693.
106 C. Liu, L. Zhang, X. Xu, J. Qiao, X. Jia, F. Wang and X. Wang, *New J. Chem.*, 2024, **48**, 13206–13213.
107 M. Faghihinezhad, M. Baghdadi, M. S. Shahin and A. Torabian, *Sep. Purif. Technol.*, 2022, **283**, 120208.
108 M. Kocijan, M. Vukšić, M. Kurtjak, L. Ćurković, D. Vengust and M. Podlogar, *Catalysts*, 2022, **12**, 1554.
109 D. Lan, H. Zhu, J. Zhang, C. Xie, F. Wang, Y. Zheng, Z. Guo, M. Xu and T. Wu, *Appl. Surf. Sci.*, 2024, **655**, 159623.
110 Z. Li, R. Mu, W. Zhang, X. Lin, Q. Cui and D. Gu, *Catal. Lett.*, 2024, **154**, 5371–5383.
111 T. Lu, H. Zhao, L. Jian, R. Ji, C. Pan, G. Wang, Y. Dong and Y. Zhu, *Environ. Res.*, 2023, **222**, 115361.
112 M. Jing, H. Zhao, L. Jian, C. Pan, Y. Dong and Y. Zhu, *J. Hazard. Mater.*, 2023, **449**, 131017.
113 H. Tang, Q. Shang, Y. Tang, X. Yi, Y. Wei, K. Yin, M. Liu and C. Liu, *J. Hazard. Mater.*, 2020, **384**, 121248.
114 Y. Chen, Y. Yu, Z. Yan, T. Li, Q. Jing and P. Liu, *Appl. Clay Sci.*, 2022, **218**, 106432.
115 Y. He, S. Zhou, Y. Wang, G. Jiang and F. Jiao, *J. Mater. Sci. Mater. Electron.*, 2021, **32**, 21880–21896.
116 D. Janardhana, S. N. Jayaramu, E. Coetsee, D. E. Motaung and H. C. Swart, *Mater. Sci. Semicond. Process.*, 2024, **184**, 108789.
117 S. Pandey, S. Kim, Y. S. Kim, D. Kumar and M. Kang, *Environ. Res.*, 2024, **240**, 117540.
118 L. Li, C. Luo, X. Chen, N. Chu, L. Li, M. Chao and L. Yan, *Adv. Funct. Mater.*, 2023, **33**, 2213974.
119 Y. Pang, Z. Tong, L. Tang, Y. Liu and K. Luo, *Open Chem.*, 2018, **16**, 401–406.
120 L. Liu, J. Fang, H. Yang, Q. Zhao, J. Deng and Y. Gou, *J. Porous Mater.*, **1380–2224**, 1573–4854.
121 H. M. Solayman, N. Y. Yahya, K. H. Leong, Md. K. Hossain, K. Kang, L. C. Sim, K.-D. Zoh, Md. B. Khan and A. Abd Aziz, *FlatChem*, 2024, **48**, 100762.
122 X. Cao, G. Liu, J. Zheng, Z. Sui, S. Zheng and Q. Zhang, *Solid State Sci.*, 2025, **160**, 107796.
123 K. Wang, C. Chen, B. Chen, Y. Wei, Y. Wang, X. Zeng, H. Yang and G. Li, *J. Alloys Compd.*, 2025, **1010**, 178326.
124 Q. Chen, L. Wu, J. Wu, K. Ma, W. Ma, W. Wu, F. Guan, P. Li, D. Liu and X.-J. Yang, *J. Environ. Chem. Eng.*, 2024, **12**, 112806.
125 K. Thangavelu, G. Abimannan, M. Altaf and Y. A. Kumar, *J. Clust. Sci.*, 2025, **36**, 56.
126 S. Merci, T. Shamspur and A. Mostafavi, *Appl. Organomet. Chem.*, 2025, **39**, e7883.
127 A. Sudha, N. Anuradha, M. Baneto, K. Ravichandran, M. Varshini, M. Ayyanar, M. S. A. Raj and I. Manimehan, *J. Mol. Struct.*, 2025, **1325**, 141013.
128 F. Bibi, M. Jamshaid, W. A. Al-onazi, A. Kalsoom, M. A. Hossain, R. Iqbal, M. S. Elshikh and S. Iqbal, *Opt. Mater.*, 2025, **160**, 116696.
129 O. Iqbal, H. Ali, N. Li, A. I. Al-Sulami, K. F Alshammari, H. S. M. Abd-Rabboh, Y. Al-Hadeethi, I. U. Din, A. I. Alharthi, R. Altamimi, A. Zada, Z. Wang, A. Hayat and M. Zahid Ansari, *Mater. Today Phys.*, 2023, **34**, 101080.
130 R. Patra, P.-C. Yang and C.-T. Hsieh, *Ceram. Int.*, 2025, **01**, 125.
131 B. Zhu, Z. Liu, N. Yu, Z. Chen and L. Zhang, *Mater. Lett.*, 2023, **335**, 133744.
132 Z. Wu, L. Yang, X. Yang, Y. Gao, X. Liu, M. Que, T. Yang, Z. Liu, H. Zheng, Y. Ma, Y. Li and J. Chen, *J. Alloys Compd.*, 2023, **940**, 168734.
133 W. Wang, X. Xin, K. An, Y. Chen, Z. Zhao, J. Tan, D. Yang and Z. Jiang, *J. Photochem. Photobiol., A*, 2022, **431**, 114045.
134 M. Kumari, N. Kumar, R. K. Sharma, S. Jain, M. Tahir, P. Singh, P. R. Makgwane and P. Raizada, *Inorg. Chem. Commun.*, 2025, **174**, 114040.
135 S. Kumar, M. N. Siddique, Md. M. Islam and S. Basu, *Mater. Chem. Phys.*, 2025, **333**, 130398.
136 P. Gotipamul, R. Maheswaran, S. Pandiaraj, S. A. Alqarni and S. Chidambaram, *Mater. Today Sustain.*, 2023, **24**, 100501.
137 G. Palanisamy, G. Venkatesh, M. Srinivasan, K. Bhuvaneswari, N. Elavarasan, S. Vignesh, T. Pazhanivel, M. Shkir, J. Hakami and J. Lee, *J. Alloys Compd.*, 2022, **922**, 166147.
138 C. Hong, W. Wang, L. Wu, J. Zhou, S. Long, W. Zhou and Y. Guo, *J. Colloid Interface Sci.*, 2025, **678**, 639–656.
139 H. Li, Y. Sun, Q. Zhang, H. Yuan, C. Dong, S. Xu and M. Xu, *Appl. Surf. Sci.*, 2023, **638**, 158010.
140 W. Xing, Y. Zhang, J. Zou, T. Zhang, C. Liu, G. Wu and G. Chen, *Int. J. Hydrog. Energy*, 2022, **47**, 12559–12568.
141 Z. Xiong, H. Hu, Z. Cao, Y. Hu, D. Sun, H. Qin and S. Kang, *Adv. Sustain. Syst.*, 2023, **7**, 2200378.

142 G. Huang, D. Zeng, P. Ke and Y. Chen, *Ceram. Int.*, 2024, **50**, 14077–14087.
143 T. Wu, Z. Liu, B. Shao, Y. Pan, Q. He, X. Zhang, L. Zhou, Y. Wang, T. Li and S. Liu, *Chemosphere*, 2024, **368**, 143731.
144 N. Li, C. Yang, H. Huang and C. Lu, *J. Build. Eng.*, 2024, **98**, 111077.
145 R. Kumar, A. Sudhaik, Sonu, P. Raizada, V.-H. Nguyen, Q. Van Le, T. Ahamad, S. Thakur, C. M. Hussain and P. Singh, *Chemosphere*, 2023, **337**, 139267.
146 T. Wang, J. Zheng, J. Cai, Q. Liu and X. Zhang, *Sci. Total Environ.*, 2022, **839**, 155955.
147 M. Mousavi, M. Hamzehloo and J. B. Ghasemi, *J. Mater. Sci.*, 2020, **55**, 7775–7791.
148 S. Amiri, F. Yazdani and H. Mortaheb, *Mater. Chem. Phys.*, 2023, **301**, 127623.
149 A. Kumar, P. Choudhary, T. Chhabra, H. Kaur, A. Kumar, M. Qamar and V. Krishnan, *Mater. Chem. Front.*, 2023, **7**, 1197–1247.
150 X. Liu, S. Chen, X. Tantai, X. Dai, S. Shao, M. Wu, P. Sun and X. Dong, *Sep. Purif. Technol.*, 2025, **363**, 132001.
151 Z.-F. Lin, T.-H. Wang, P. Venkatesan and R.-A. Doong, *Chem. Eng. J.*, 2025, **505**, 159411.
152 P. Wang, L. Wang, L. Rao, J. Shao, Q. Yuan and S. Shan, *J. Environ. Manage.*, 2025, **377**, 124692.